UNIVERSITY OF CAPE TOWN
IYUNIVESITHI YASEKAPA • UNIVERSITEIT VAN KAAPSTAD

TECHNICAL REPORT

CRU-BM-2010-01

PROCESSING AND CHARACTERISATION OF POLYMERIC BIOMATERIALS FOR TISSUE ENGINEERING AND REGENERATION

L. Bruchmueller, H. Krynauw, D. Bezuidenhout, T. Franz

Biomechanical Sciences
Cardiovascular Research Unit
University of Cape Town

August 2010

I Table of Contents

II List of Figures

III List of Tables

IV Glossary

KIT	Karlsruhe Institute of Technology
UCT	University of Cape Town
CVRU	Cardiovascular Research Unit
ECM	Extracellular Matrix
TIPS	Thermally Induced Phase Separation
SIPS	Solvent Induced Phase Separation
SEM	Scanning Electron Microscope

V Nomenclature

E	linear elastic modulus
ε_{elast}	strain at linear elastic limit
ε_{max}	strain at maximum stress
σ_{elast}	stress at linear elastic limit
σ_{max}	stress at maximum
σ_1	maximum stress of precycle 1
σ_2	maximum stress of precycle 2
σ_3	maximum stress of precycle 3
σ_4	maximum stress of precycle 4
σ_5	maximum stress of precycle 5
σ_6	stress at 20% elongation of original gauge length (L_0) in final tensile testing to failure

Chapter 1 Introduction

Currently, heart diseases are the leading cause of death in the United States [1]. Frieden showed that the increase of these chronic diseases is caused by the modern western lifestyle [2]. As developing countries are adopting the western lifestyle, the percentage of worldwide mortalities caused by cardiovascular diseases is expected to increase [3, 4].

Heart diseases can frequently be connected to atherosclerosis, which leads to a reduced capacity of vessels to transport blood. If the patient is not suited to treatment by intravascular stenting, this is commonly treated by autologous grafting - the surgical bypassing of the affected vessel with a vessel taken from another part of the body [5]. In about one third of those cases, autologous vessels are not available as the suitable vessels have been used before, or might have pre-existing diseases [6]. Patients whose vessels cannot be bypassed then face palliative medical therapy and often suffer heart attacks or amputations as the blood flow is increasingly constricted [5]. This leads to the need for non-autologous grafting in the form of prosthetic vascular grafts.

The Cardiovascular Research Unit (CVRU) at the University of Cape Town (UCT) is researching a variety of synthetic artery concepts, including the biomechanical modelling of the structural behaviour of synthetic electro-spun grafts. This computational study will be combined with in vitro testing to optimize the design of the graft. The aim is to produce vascular grafts combining an electro-spun micro-fibrous mesh with a compliant reinforcement structure. Both the micro-fibrous layer and the reinforcement structure are made of polymers that will hydrolytically degrade in the aqueous surroundings of the body. The micro-fibrous layer allows in-growth of human tissue and the reinforcement structure increases the mechanical strength.

The present study focuses on the characterisation of the mechanical properties of degradable electro-spun vessel walls at various stages of *in vitro* degradation. This information will be important for the computational biomechanics research on electro-spun vascular grafts, as the change in mechanical properties affects the structural stability of the graft. To provide structural stability, the decrease of mechanical strength needs to be proportional to the regrowth of new tissue, otherwise drawbacks in function can occur [7].

This thesis will present the state of knowledge concerning required properties and fabrication of vascular grafts. Based on this knowledge the experimental methods for electro-spinning and the testing procedure will be set up. The results will be reported and analysed, after which conclusions and recommendations will be given.

Chapter 2 State of prior art

2.1 Introduction

This part of the thesis will explain the medical and technological constraints for the fabrication of vascular grafts.

The ultimate goal in the overall project is the development of degradable vascular grafts which allow an overall integration and healing to give long term patency. The mechanical properties of the graft influence this healing pattern and the replacement vessel needs to mimic the mechanical properties of a human blood vessel to provide mechanical functionality. Therefore, in section 2.2 and 2.3 the mechanical properties of blood vessels and the medical requirements for grafts will be explained. In section 2.4 - 2.7 the focus will be on fabrication techniques in order to choose the one which best suits the needs.

2.2 The human artery

2.2.1 Structure and function

The healthy human vessel wall consists of three layers of different thickness [5].

- The innermost layer (intima) consists of endothelium on the inner side, and of internal elastic lamina on the outer side. The endothelial layer is a single cell layer that prevents spontaneous blood clotting in the vessel and regulates vascular smooth muscle cell tone. The elastic lamina consists of elastic fibres which enable the vessel to stretch, and allow transport of nutrients and waste.
- The second layer (media) is bounded by the internal and external elastic lamina on each side. It is composed of numerous layers of aligned smooth muscle cells and extracellular matrix. It contributes the bulk of the mechanical strength to the vessel as well as its compliance – its ability to stretch radially. It can also contract or relax in response to external stimuli and by this change in its compliance.
- The outer layer (adventitia) is composed of external elastic lamina on the inner side and the outer surface of the artery on the outer side. The outer surface consists primarily of fibroblasts and extracellular matrix which provide the ultimate

mechanical strength, and harbours the microscopic blood supply of the artery as well as its nerve supply.

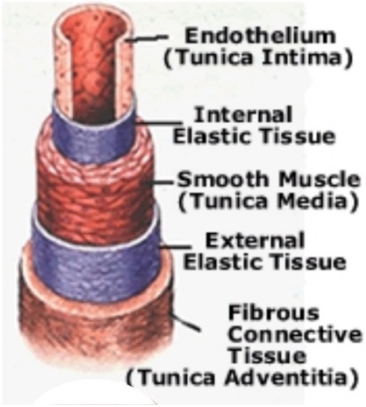

Figure 2.1 The layers of arteries [8]

For vascular grafting, the radial compliance is an important parameter to determine and control [9]. As the cardiovascular compliance is provided by the medial layer [10], arterial tissue engineering aims to mimic the properties of this layer. Depending on the surface structure and material of the mimicked medial layer, the body is able to build up the endothelial layer on the lumen[1] and the blood supply of the artery on the ablumenal[2] side [11, 12].

2.2.2 Strategy of the CVRU

The strategy of the CVRU is to mimic the medial layer with an electro-spun micro-fibrous mesh and the adventitia of arteries with a compliant reinforcement structure. The electro-spun micro-fibrous mesh enables tissue regeneration whilst the reinforcement structure adds mechanical stability. The combination of the electro-spun micro-fibrous mesh and the reinforcement structure forms the vascular graft. To design the compliance of the whole graft, both components need to be characterised. This study is limited to the mechanical characterization of the electro-spun mesh and the changes occurring as the mesh degrades.

[1] The inner surface of a blood vessel
[2] The outer surface of a blood vessel

2.3 Requirements for a functional degradable graft

2.3.1 Biocompatibility

The biocompatibility of a graft is related to its interactions with the body. A biocompatible graft should not be excessively toxic, inflammatory, or thrombogenic either in itself, or by release of toxic, inflammatory or thrombogenic additives or degradation products [13]. To enable tissue regeneration, the graft also needs to support the attachment, proliferation and migration of the desired cell types. The characteristics described above are mainly influenced by the porosity [14], the structure and the chemistry of the surface. For example [15]:

- Different cell types attach to different surface structures. In general it was found that osteoblasts prefer a rougher surface, fibroblasts attach better to a smoother surfaces and epithelial cells attach only to the smoothest surfaces.
- Differences in the chemistry of the outermost functional groups of a surface affect endothelial cell attachment and proliferation. However the exact mechanism is not clear [16]. Therefore each material needs to be examined to determine if it will allow the growth of an endothelial layer.

The structure and the chemistry of the surface thus need to be adapted for each application. To enable vascular grafting, the structure needs to support the in-growth of smooth muscle cells [7], the growth of the endothelial layer on the inner side and the formation of the blood and nerve supply on the outer side of the graft.

2.3.2 Provision of a temporary extracellular matrix

Healthy organs are composed of various cell types and an extracellular matrix (ECM). The ECM is a highly porous interlocking mesh of fibrous proteins and glycosaminoglycans. Tasks of the ECM are [7]:

- Definition of the shape of the organ;
- Provision of structural stability;
- Provision of a scaffold on which the cells can proliferate and migrate. This scaffold also serves as space-holder which prevents damage of growing cells and allows incorporation of biological or mechanical signals to enhance tissue formation;

- Provision of a pore branching network for the diffusion of nutrients, oxygen and wastes;
- Function as a delivery vehicle for cells towards regions where new tissue growth is desired.

Cardiovascular tissue engineering aims to mimic the ECM-structure of arteries in order to enable the desired cell types to attach and proliferate in the mesh-like structure and by this fill the spaces between the fibres [7]. The artificial ECM provides primary mechanical stability while the cellular structure matures. As the scaffold begins to degrade, a natural ECM is formed and the newly regenerating cells are gradually loaded with physiological stress due to pulsatile flow. Eventually the scaffold completely degrades and the regenerated tissue bears the stress [17].

2.3.3 Biodegradability

Biodegradation is based on the premise that the original material is slowly broken down into small, non-toxic molecules which are soluble in water and can therefore be excreted through the kidneys [18].

This degradation process can happen in two different ways:

1) Enzymatic degradation by human enzymes:
   Most of the naturally occurring polymers contain enzymatically sensitive bonds and hence undergo enzymatic degradation. Natural polymers like collagen, elastin or fibrin can be considered as the first biodegradable biomaterials used clinically. However, the precise design of enzymatically degradable grafts with controlled degradation speed is complicated. The *in vivo* degradation rate of enzymatically degradable polymers varies significantly with the site of implantation depending on the availability and concentration of the enzymes. Chemical modification of these polymers can also significantly affect their rate of degradation [19].

2) Hydrolytic degradation in the aqueous surrounding of the body:
   Hydrolytically degradable polymers have hydrolytically labile chemical bonds such as esters, orthoesters, anhydrides, carbonates, amides, urethanes, ureas, etc. [20] in their backbone. The degradability of a material is also connected to its hydrophilic properties which enable the water molecules to attach to the material and subsequently

split the linkages. However, most polymers are mainly hydrophobic due to their non polar components. To achieve better hydrophilic properties hydrophilic components can be incorporated in the polymer [21].

Hydrolytic degradation occurs in two steps: First, the macromolecular chain is broken by random hydrolytic cleavage while the sample mass remains unaltered. When the chain fragments reach a critical size, mass loss can be observed and the second step of degradation starts. The mass loss is associated with polymer fragments small enough to permeate out of the polymer bulk into the aqueous medium [22].

When designing the graft, its degradation speed needs to be controlled in order to be proportional to the re-growth of new tissue, otherwise drawbacks in function can occur: If the degradation speed is too high, growing cells can be loaded too early and therefore damaged; if the degradation speed is too low, growing tissue is not strengthened during development and hence more susceptible to injury later on. Thus, controlling the mechanical strength of the degrading graft versus time is extremely important and challenging [7]. As hydrolytically degradable polymers show minimal site-to-site and patient-to-patient variations compared to enzymatically degradable polymers, their degradation rate can be controlled more easily and they are generally preferred as implants [19].

2.3.4 Hydrophilic properties

Hydrophilic properties of grafts are essential for several reasons. As mentioned above they enable the hydrolytic degradation of the graft. In addition, hydrophilic properties are necessary to create a positive host response of the body towards the implant. As the body is an aqueous environment the graft should be hydrophilic to be accepted by the body and to enable the transport of nutrients and waste [21].

2.3.5 Summary of the requirements for degradable vascular grafts

Summing up the requirements on vascular grafts, the task in cardiovascular tissue regeneration is to find a degradable and sufficiently hydrophilic material which is able to form a structure which mimics the extracellular matrix of the desired cardiovascular tissue. It must also form a surface structure which supports the growth of the desired cell type and have functional groups which enable the endothelial layer to build up.

2.4 DegraPol®

For medical applications, materials are needed in which the degradation rate and the mechanical properties are independently adjustable to the medical needs [23]. Based on hydrolytic degradation and with special consideration of the medical requests described above, a copoly(ester-urethane), termed DegraPol® (AB Medica SPA, Lainate, Italy), was developed [24]. The CVRU is working with DegraPol® since this material fulfils the medical requirements described in Section 2.2 and 2.3, and also enables the adjustment of the mechanical properties and the degradation.

DegraPol® is a phase-segregated multiblock copolymer built up by co-condensation of two macrodiols, a crystallizable hard segment (poly{3-(R-hydroxybutirrate)-co-(?-caprolactone)}-diol) and a non-crystallizable soft segment (polycaprolactole-dyglicole-diol), coupled with a diisocyanate. The amorphous soft domain forms a continuous matrix in which the crystals are dispersed. The mechanical properties of such block copolymers are determined predominantly by the content of crystallizable segments, but are little influenced by the chemical structure and the composition of the amorphous segment [23]. This copolymer can be made degradable by insertion of weak links in the form of easily hydrolyzable glycolyl-glycolate ester bonds into the macrodiols [25].

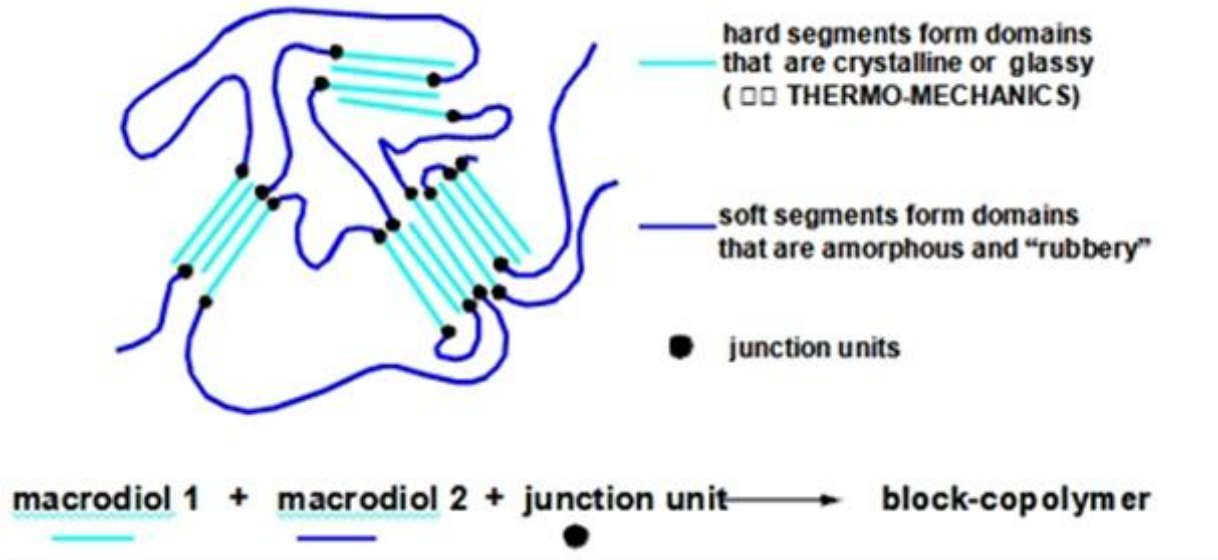

Figure 2.2 Non-degradable DegraPol® structure [26]

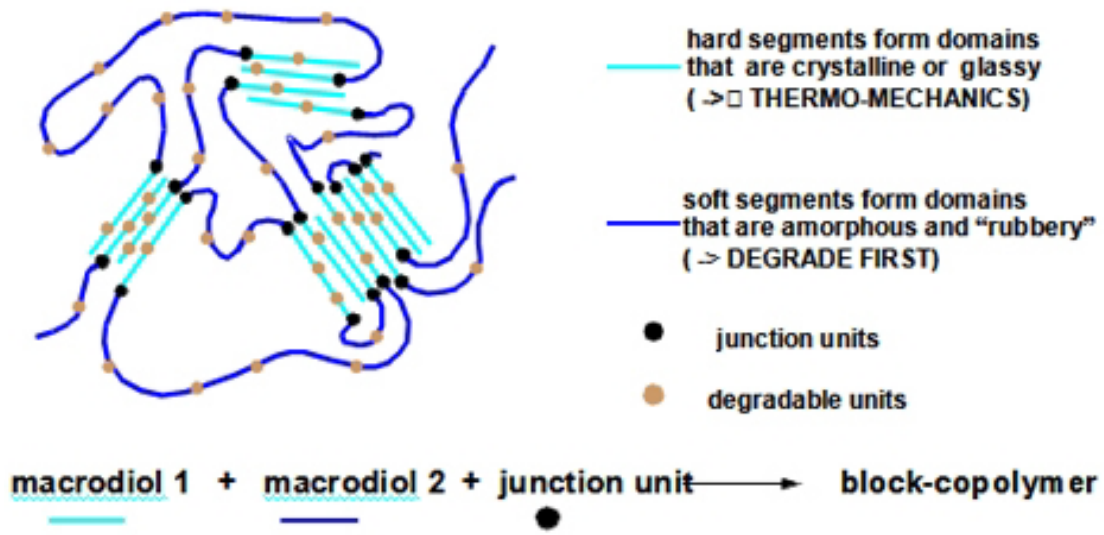

Figure 2.3 Degradable DegraPol® structure [26]

By using different ratios of hard and soft segment, it is possible to modulate the mechanical properties of the final product. For example, the elastic modulus of the bulk material DegraPol® is adjustable between 50 MPa and 500 MPa [23]. The hydrolytic degradation rate can be controlled by the amount and the sequence distribution of the easily hydrolyzable glycolyl-glycolate ester bonds and can vary between several weeks and several years [23]. The suffix of DegraPol® materials expresses the ratio of hard segments, soft segments and easily hydrolyzable glycolyl-glycolate ester bonds. DegraPol® is biocompatible [25] and its degradation products are non-toxic. It was shown that DegraPol® in vivo evokes a cellular and angiogenic response that is dictated by architecture: Increasing scaffold porosity promotes angiogenesis and cellular infiltration [11, 27]. DegraPol® surfaces have been tested for hemocompatibility with fresh human whole blood and it was shown that the complement system is moderately activated in a comparable manner to clinically used materials, the blood clotting cascade is not induced and platelet adhesion increased in a comparable manner to clinically used materials [12].

2.5 Processing techniques

Once the decision about the material is made, there are a number of different processing possibilities like electro-spinning, winding, weaving, dip-coating, spraying and extruding [13]. These techniques have an important influence on the mechanical properties of the resulting graft. This review will describe the three mainly used structures and their applicability for grafting:

- **Films** can be produced by solvent casting and form non porous scaffolds [28]. Due to their non porous structure they cannot facilitate the transport of nutrients and oxygen to the cells and are thus not suitable for cell scaffolding. Apart from that they are mechanically too brittle for dynamic applications [21].
- **Foams** can be produced by thermally or solvent induced phase separation (TIPS/SIPS). In this fabrication technique the frozen polymer solution is treated under vacuum to evoke the sublimation of the solvent. This process manufactures a structure which is suitable for tissue engineering as it provides high porosity and large diameter interconnected pores which can facilitate cell seeding and transfer of oxygen and nutrients [29]. The problem of this process is the lack of precise control over scaffold specifications like pore size, shape, distribution and interconnectivity of the pores as well as the overall scaffold shape. Since the pore size is crucial for cell growth, this is a big handicap for tissue engineering applications [7].
- **Meshes** can be produced by electro-spinning and possess morphologies and porosities which mimic the ECM and are therefore excellently suitable for tissue engineering [7, 30]. The highly porous nature of an electro-spun micro/nano-fibrous matrix allows for cells migration and growth as well as transport of nutrients and waste. Depending on the polymers which are used, electro-spun meshes show linear elastic behaviour and high deformation at break. These properties enable them to be applied both in dynamic culture experiments and for tissue engineering of especially soft tissues, thus overcoming problems related to the relative inflexibility of traditional polyester scaffolds [31, 32].

All of the structures described above have already been processed with DegraPol® [33], [31], [22], however, the structure influences the possibilities of application. DegraPol® foams were used for comparably stiff applications like bone formation [33], whilst meshes are most

suitable for soft and cyclically loaded applications like cardiovascular tissue [31, 32]. This project will examine electro-spun DegraPol® meshes.

To produce meshes with optimal properties for the intended application it is important to understand the process of electro-spinning. Knowing its technical details, adjustable parameters and limitations is required to develop an idea of the structures that can be spun. The following section will describe the process of electro-spinning.

2.6 Electro-spinning

2.6.1 Basic technique

Electro-spinning is based on the following principle: When a strong electrostatic field is applied to a drop of polymer solution held at the tip of a syringe needle or capillary, the droplet will start to deform into a conical shape known as a Taylor cone [34]. As the electrostatic force overcomes the surface tension of the drop, a liquid jet will be ejected and pulled towards the nearest electrically earthed surface. As the solvent evaporates from the jet, the viscosity increases until the jet dries and solidifies, and a micro/nano-fibre is formed. If the collector is a flat plate, the fibres will form a non-woven sheet spread on the collector because of residual charges which repel arriving fibres. If the collector is a cylinder rotating around its own axis, a cylindrical conduit consisting of partially aligned fibres will form. By translating the cylinder along its axis, a longer cylindrical conduit can be produced. An electro-spinning setup like this is shown in Figure 2.4. The drop size of polymer solution at the tip of the syringe is kept constant by pumping it at a constant flow rate by means of a syringe pump [34].

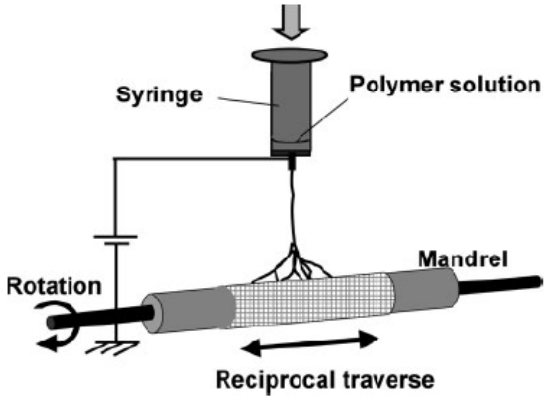

Figure 2.4 Electro-spinning setup Fig.1 in [35]

When leaving the Taylor cone the jet has a relatively large diameter and becomes thinner as the electrical forces accelerate the polymer liquid so that the mass per unit time passing any point of the axis stays constant. The jet travels in a straight line for some distance in the direction of the applied electric field. Beyond that distance, the path is curved. The behaviour of the jet changes according to the changes in volume, density and viscosity, which occur as the solvent evaporates and the temperature changes [34].

2.6.2 Relationship between spinning parameters and results in structure

Regarding the process described above there are many different parameters which influence the result of the spinning process. These parameters can be classified in three groups [36]:

- **Controlled variables** (electric field strength, flow rate, solution concentration, solvent boiling point, distance between tip and collector, collector composition and geometry,)
- **Solution properties** (viscosity, surface tension)
- **Ambient parameters** (Temperature, humidity)

The solution properties are complex to adjust as they are interdependent: Once the material is chosen, the set of solution properties is selected and can be influenced by ambient parameters or controlled variables:

Electrical field strength: The electrical field is given by the potential difference between the tip of the needle and the collector, divided by the distance from the tip to the collector (V/distance). To overcome the surface tension and form a fibre a minimum threshold voltage is required. As the electric field strength increases, the fibre travelling through the air is accelerated and shows a rougher surface [37]. If the voltage increases even more, several fibres can form at the tip of the Taylor cone.

Flow rate: the flow rate can be determined by the pumping rate but may oscillate slightly with time as the shape of the droplet varies, even if a constant flow rate is being pumped.

Solution concentration: By changing the proportions of solvent and polymer the viscosity changes as well as the surface tension. As the solution becomes more viscous, the minimum required potential difference increases because more force is required to overcome the surface tension to form the jet. Below a critical concentration, and therefore viscosity, stable jet formation becomes difficult as the jet breaks down. Above a critical viscosity stable jet

formation also ceases [36]. Changes in temperature also influence viscosity and surface tension.

Solvent boiling point: By choosing another solvent the solvent boiling point can be altered. The higher the boiling point of the solvent, the slower it evaporates. If insufficient evaporation occurs before the jet reaches the collector, the fibres will merge and form a solid film, thereby losing its bio-scaffold characteristics. If the fibres only merge at certain contact points with other fibres, the mesh will be more rigid, thus exhibiting increased mechanical strength and durability [35]. The amount of merging that takes place can also be influenced by ambient conditions like temperature, humidity and air velocity in the electro-spinning chamber [36].

Distance between tip and collector: A comparably small distance (around 10 cm) produces more constant fibre diameters than a larger distance (20 or 30 cm), but at the same time the distance has to be large enough for the solvent to evaporate before reaching the collector. Depending on the polymer solution and the application, a suitable compromise must be made [7].

Collector composition and geometry: As described in section 2.6.1 the collector composition and geometry influences the orientation of the resulting fibre sheet. The use of a flat plate results in a non-woven sheet spread, whilst a cylindrical collector rotating around its own axis will form a cylindrical conduit consisting of partially aligned fibres. Alignment and diameter of the fibres can be influenced by the rotation speed. A higher rotation speed of the cylinder results in more aligned and thinner fibres.

To ensure a reproducible and consistent spinning process, a stable Taylor cone is required. The formation of a stable Taylor cone is mainly influenced by the coordination of the voltage and the flow rate. Depending on the viscosity of the polymer and solvent, the right combination of voltage and flow rate must be found.

2.6.3 Desired characteristics of electro-spun grafts

The outstanding advantage of an electro-spun fibre is superior mechanical behaviour compared to bulk material. Due to their molecular orientation, electro-spun fibres show significant higher elastic modulus and strength than extruded fibres [7, 32]. The precise mechanical properties are highly dependent on the morphology of the fibre. It is known from

materials science that a stressed cylinder/fibre experiences locally increased stress and therefore a higher possibility of failure if the diameter changes suddenly. The most consistent mechanical strength of the single fibre - and subsequently the electro-spun mesh - is achieved with a constant fibre diameter.

As mentioned above the amount of merging also influences the stiffness, mechanical strength and durability of the electro-spun mesh [35]. Depending on the material and the intended application the amount of merging needs to be adjusted.

2.7 Previous studies on electro-spun grafts

2.7.1 Electro-spun DegraPol® meshes

So far several studies focussed on electro-spun DegraPol® [11, 12, 31]. In all of these studies, the solvent chloroform (CHCl3) was used and polymer-chloroform solutions of 25-30 weight% were produced. For the spinning process voltages between 18 and 20 kV and a spinning distance in the region of 200 mm were applied. The resulting meshes showed fibre thicknesses in the range of 10-20 □m. However these studies focussed more on the investigation of the medical compatibility and less on the mechanical properties [11, 12].

Data about mechanical properties of electro-spun DegraPol® reports linear elastic behaviour up to 10% deformation, tensile modulus E of 10.15±0.69 MPa and deformation at break higher than 200% [31]. These values refer to the freshly spun mesh and might vary depending on the structure of the electro-spun mesh and the state of degradation.

With regard to cyclic applications, preconditioning needs to be taken into account. When loaded cyclically, some materials change properties to adapt to the cyclic stress. To determine the mechanical properties of the material for cyclic applications, tensile precycles can be done before tensile testing to failure [31].

In previous studies it was shown that cyclically loaded elastomeric materials can show a characteristic similar to the “Mullins effect” [38]. This effect can be described as an instantaneous and irreversible softening of the stress-strain curve that occurs whenever the load increases beyond its prior all-time maximum value. At times when the load is less than a prior maximum, nonlinear elastic behaviour prevails. A corresponding stress-strain curve is shown in Figure 2.5. This phenomenon has also been seen in electro-spun polycaprolactone

[39] and electro-spun polyurethane mats [40]. As the current study works with an electro-spun elastomer, a similar behaviour can be expected for cyclic tensile loading.

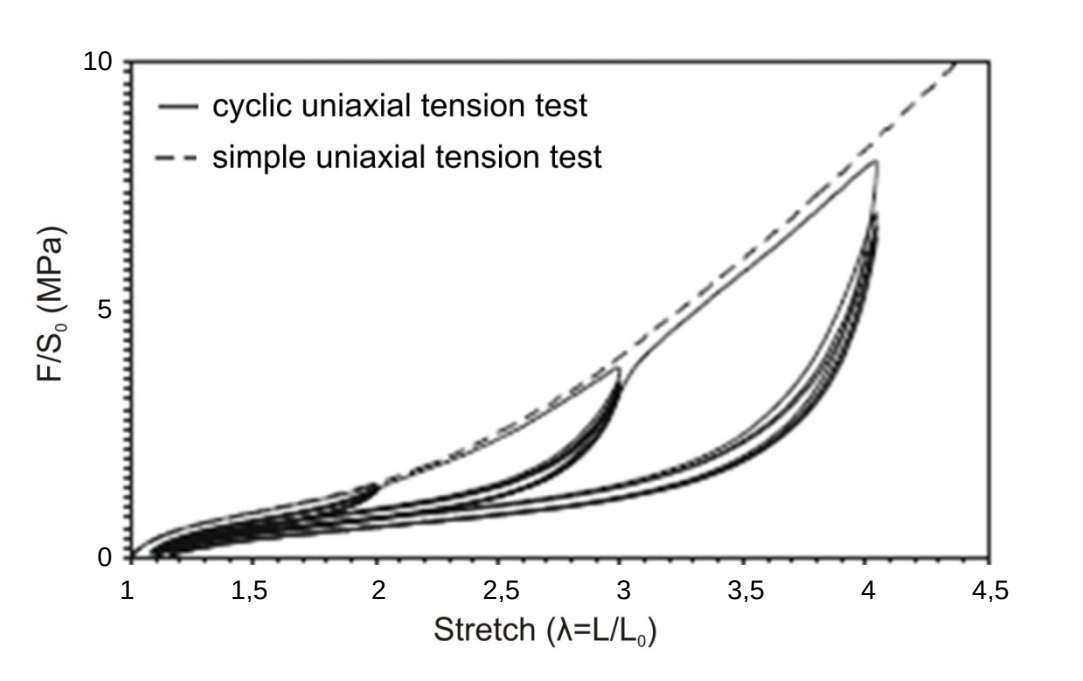

Figure 2.5 Stress-strain response of a material exhibiting the Mullins effect [38]

2.7.2 Degradable vascular grafts

Numerous studies have independently evaluated the challenges of developing mechanically suitable vascular grafts and non-thrombogenic blood contacting surfaces [41]. So far several degradable vascular scaffolds have been developed based on a variety of hydrolytically labile polyesters [42]. Many of these scaffolding materials are naturally stiff and lack the ability to match the compliance of the native vessels [31, 41]. Therefore just a few degradable electro-spun vascular grafts have been processed successfully. These grafts were made of fibrinogen [32] and a blend of polyglyconate (Maxon) and proteins such as gelatin and elastin [43]. However, the degradation rates of fibrin, gelatin and elastin are difficult to control as they are enzymatically degradable polymers. Another successful vascular graft was produced by electro-spinning a blend of biodegradable poly(ester urethane)urea and non-thrombogenic bio-inspired phospholipid polymer, poly(2-methacryloyloxyethyl phosphorylcholine-co-methacryloyloxyethyl butylurethane) [41]. Poly(ester urethane)urea and DegraPol® (Poly(ester urethane)) are very similar, however DegraPol® is a ready to use material with adjustable degradability and tunable mechanical strength. This encourages the use of DegraPol® for vascular grafting.

2.8 Summary

No reference has been found about degradable vascular grafts made of DegraPol®. It was shown that DegraPol® is suitable for grafting [11, 12, 25, 27]. Processing DegraPol® by electro-spinning allows cyclic applications like cardiovascular tissue regeneration. However, in order to apply DegraPol® grafts for cardiovascular operative interventions, the mechanical strength of the degrading graft versus time needs to be determined and controlled [7].

The current study will examine the change in the mechanical behaviour of electro-spun DegraPol® grafts during degradation. The spinning parameters will be kept similar to previous studies to ensure that the structure allows cell attachment and proliferation as well as comparability of the results [25].

Chapter 3 Materials and methods

3.1 Electro-spinning

For the spinning process, the electro-spinning rig of the CVRU was used. Before spinning the samples, further developments were made on the existing rig. The following sections will describe the original state of the rig, the changes that were done and the parameters applied for spinning.

3.1.1 State of the spinning rig

The electro-spinning rig of the CVRU (see Figure 3.1) consists of a box connected to an extractor hood, an ammeter, a syringe pump and a 0-30 kV power supply which is connected to a charged needle and an earthed collector. The earthed collector is a rotating mandrel which is fixed on a translating platform which is driven by means of a stepper motor.

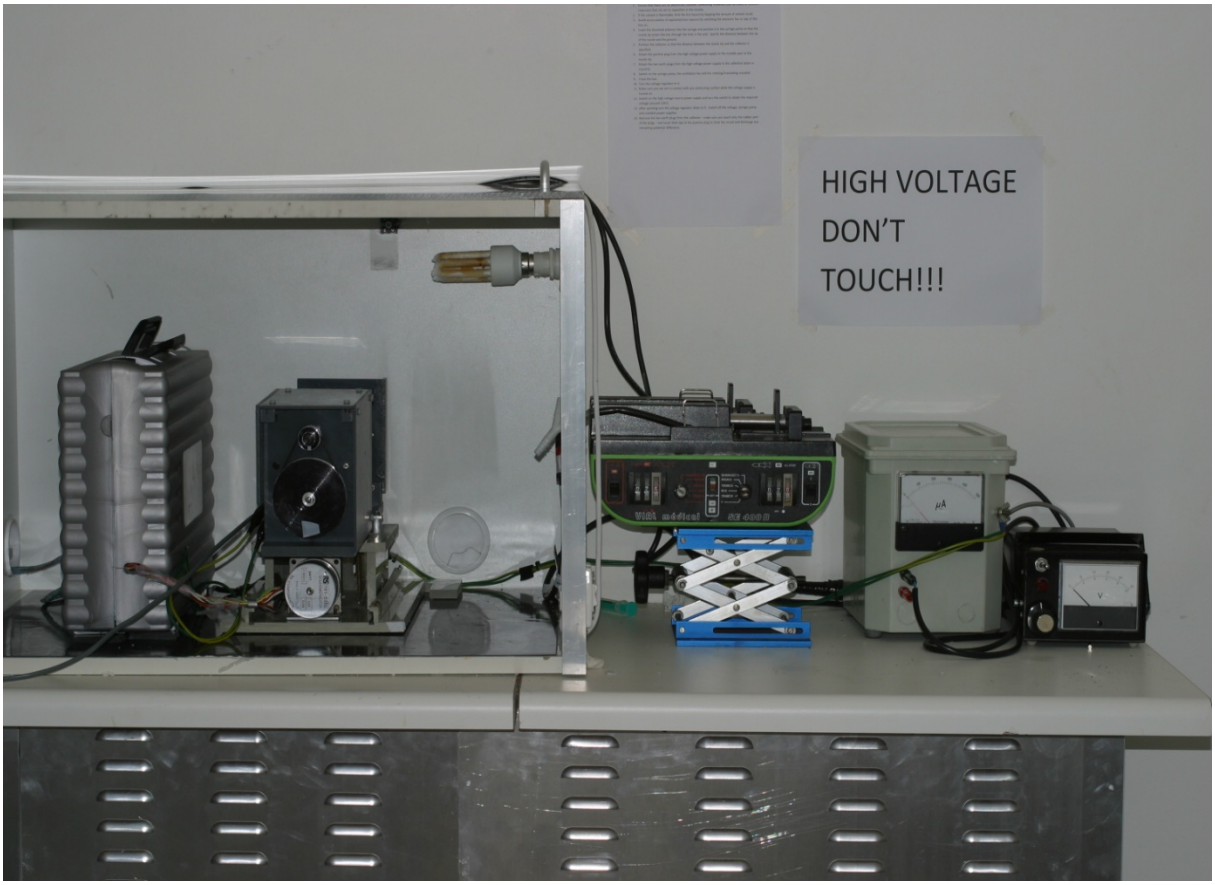

Figure 3.1 Photograph of the complete electro-spinning rig

Problems during the electro-spinning process:

- The motor turning the mandrel was overloaded, turned hot and stopped working;
- The rotation speed of the mandrel was uneven and could not be controlled;
- The mandrel was not supported at the free end, thus it vibrated during rotation;
- The mandrel could not be exchanged with mandrels of different diameters;
- Many fibres went to the wall of the box instead of going to the mandrel;
- The stepper motor translating the mandrel worked unreliably.

3.1.2 Further development of the spinning rig

To ensure a constant and reproducible spinning process, the existing electro-spinning rig was modified. The basic setup, as it is described above, was kept whilst the whole platform with the collector was exchanged (see Figure 3.2, Figure 3.3 and Figure 3.4). The newly built collector differs from the previous one in several ways:

- It has a 74 W brushed DC motor with a 4:1 pulley ratio enabling rotation speeds up to 10000 RPM;
- The mandrel is held by a chuck which can be adjusted to different mandrel diameters;
- The end of the mandrel is supported radially.

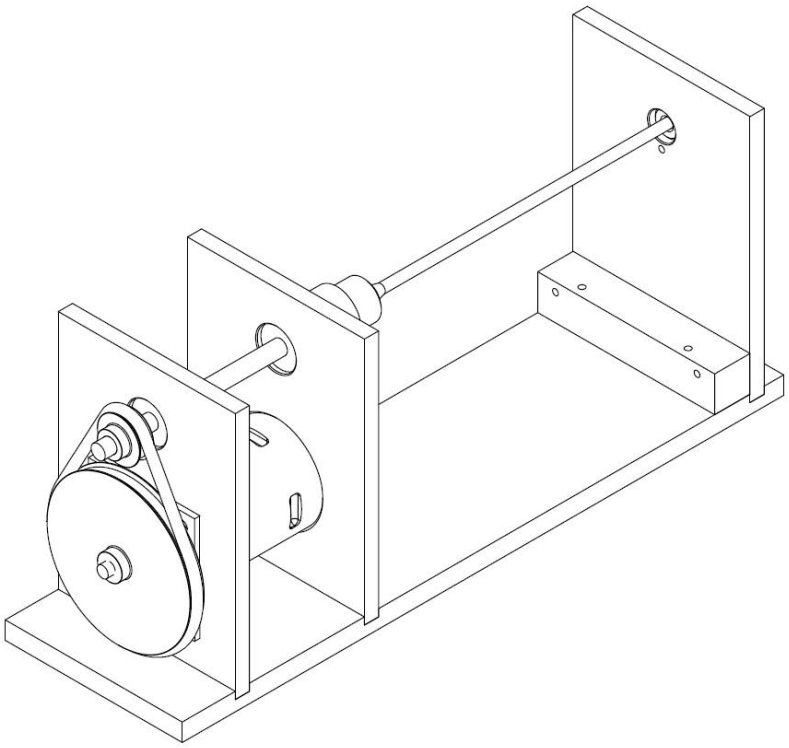

Figure 3.2 Technical drawing of the improved spinning rig

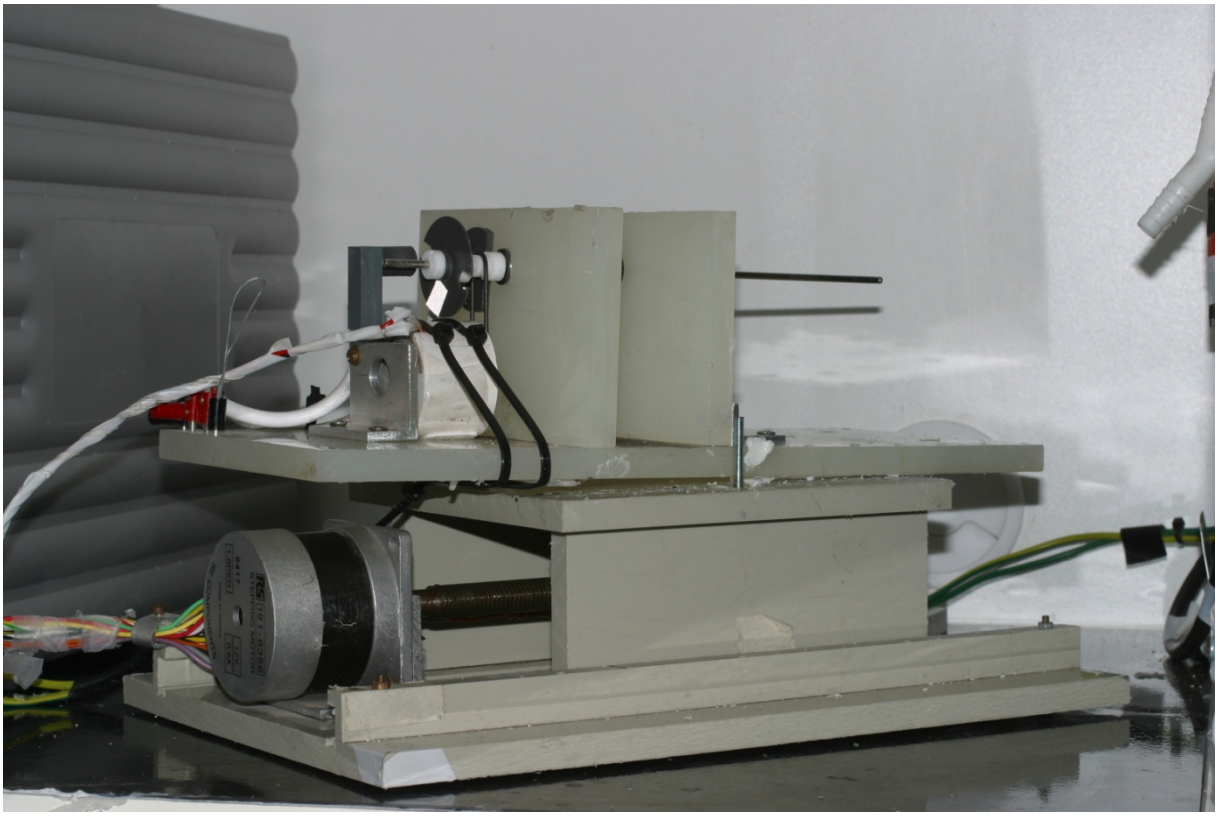

Figure 3.3 Photograph of the collector, original spinning rig

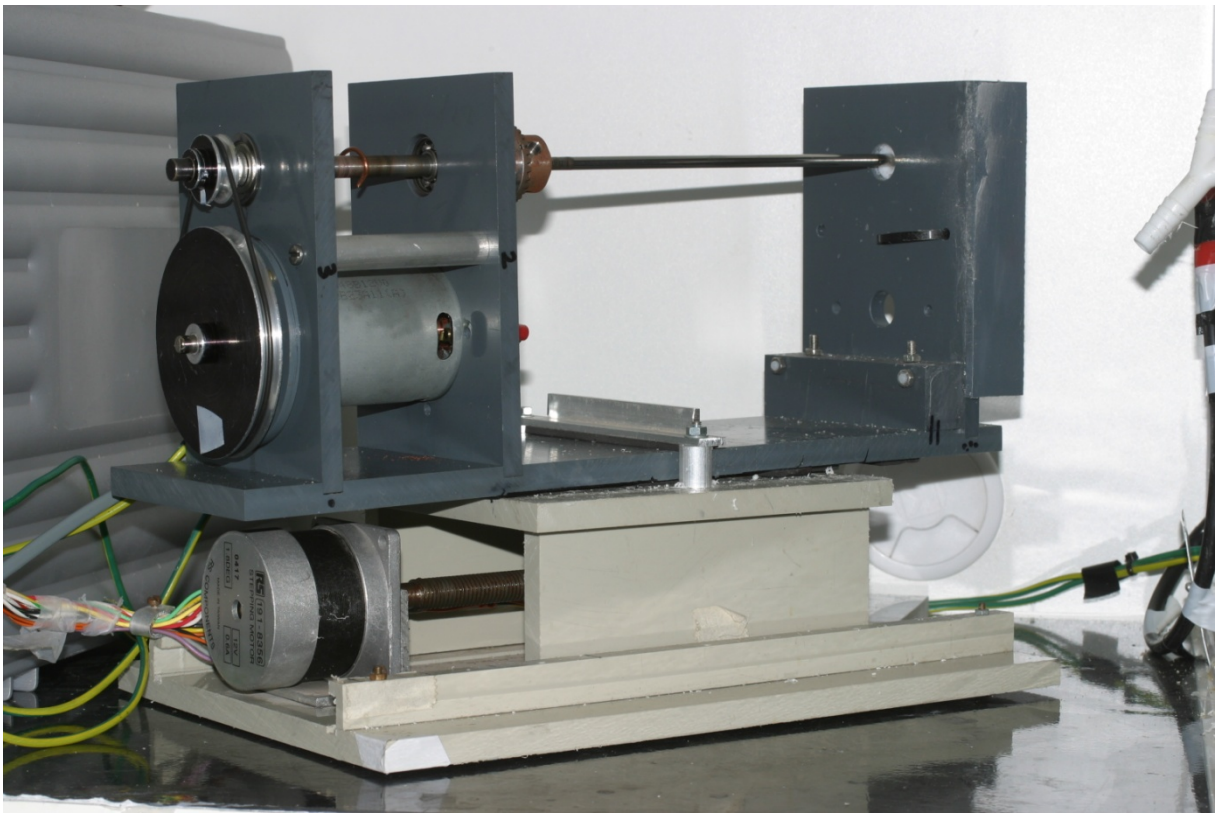

Figure 3.4 Photograph of the collector, improved spinning rig

Another modification was done in the polymer charging region: The syringe needle was put through a metal plate with a centred hole. This metal plate was charged together with the polymer solution to give a focus to the jet and prevent spinning towards the walls of the box. The conduction of the changes described above was part of another project.

The samples for this project were spun using the improved spinning rig.

3.1.3 Parameters for manufacturing scaffolds

Twenty weight percent (20 w%) DegraPol® D30 was dissolved in Chloroform (CHCl3). The polymer solution was sonicated at 37°C for 90 minutes and then spun at room temperature with a flow rate of 1.437 ml/hour and a voltage of 13 kV. While spinning, the mandrel rotated at 4000 RPM and translated 95mm with 2.6 mm/s. The distance of the needle tip and the collector was 200 mm. For each graft 1.5 ml of the polymer solution were used.

3.2 Graft removal from the mandrel

Based on the parameters described above, 8 grafts were spun. After finishing the spinning process, each of the grafts was soaked in ethanol for 5 minutes, then cut open lengthwise, peeled off the mandrel and dried under vacuum to avoid possible transesterfication. Due to the decreasing wall thickness towards the ends of each graft, 1-2 cm of the graft length was cut off on both sides. The remaining part of the graft was used to prepare the samples.

3.3 Sample preparation

Three different types of rectangular sample strips were cut from the grafts:

Name	Sample width	Sample purpose	Amount of samples
C	10mm	Circumferential tensile testing	45 samples randomized over all grafts
W	10mm	Determination of mass loss	1 sample per graft
S	3 mm	Structure analysis with the Scanning Electron Microscope (SEM)	10 samples (1 per graft + 2 for different degradation time points)

Table 3.1 Sample preparation plan

Each sample is named by 3 variables: Sample name, graft number – sample number.

The sample numbering of each graft started on the side of the chuck and increased towards the other end. The first sample on each graft was the *S* sample; two grafts had another *S* sample, then the *C* and *W* samples were randomized on the remaining length of each graft. As an example of the sample characterisation, Figure 3.5 shows the cutting plan of graft 5:

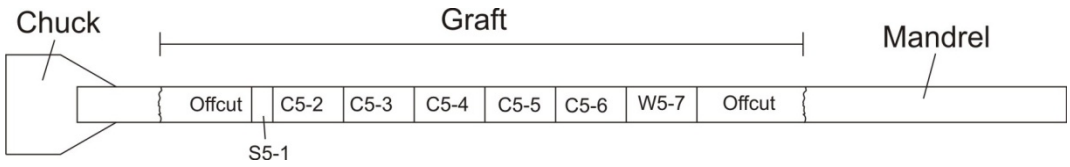

Figure 3.5 Cutting plan of graft 5

3.4 Hydrolytic degradation

Depending on the type of sample, different degradation plans were set up, which will be explained in the following sections.

3.4.1 Degradation of *S* samples

One *S* sample of each graft was analysed using the Scanning Electron Microscope (SEM) without any degradation. The two extra *S* samples were positioned in separate sample tubes which were filled with 0.66 ml of distilled water and kept in the incubator at 37 °C for 14 or 34 days, respectively. After the desired time of degradation, the samples were taken out of the water and dried under vacuum at room temperature to stop the degradation process and to be analysed using the SEM.

3.4.2 Degradation of *C* samples

The *C* samples were split up in 9 groups which contained 5 samples each. Each group was degraded for a different period of time. The samples of the first group served as undegraded control, whilst each sample of the other groups was placed in a separate sample tube which was filled with 2 ml of distilled water and kept in the incubator at 37 °C. One group was removed after each time interval of 5, 10, 14, 18, 22, 26, 30 and 34 days of hydrolytic degradation. All samples of the removed group were taken out of the water and dried under vacuum at room temperature to stop the degradation process. The size and the tensile properties of all samples were measured.

3.4.3 Degradation of *W* samples

After an initial mass measurement, each *W* sample was positioned in a separate sample tube, which was filled with 2 ml of distilled water and kept in the incubator at 37 °C. After 5 days of hydrolytic degradation, all samples were taken out of the water and dried under vacuum at room temperature. The mass of the dry samples was measured. Following this, each sample was put back into its original tube with the previous water to continue degrading in the incubator at 37°C. This process was repeated after 10, 14, 18, 22, 26, 30 and 34 days of degradation.

Before and after the degradation process, all samples were kept dry in a desiccator with silica gel to avoid degradation by the moisture in the air.

3.5 Sample characterization

3.5.1 Microscopic structure

All *S* samples and 2 *C* samples (after tensile testing to failure) were sputter coated with gold in a Polaron SC7640 and analysed using a JEOL JSM5200 scanning electron microscope with 25 kV and WD = 48. Micrographs of the cut region, the inner and the outer surface were taken to determine surface structure and fibre alignment.

3.5.2 Mass

To determine the mass of the *W* samples, each sample was weighed 3 times on a Mettler Toledo XS105S scale. To calculate the mass loss of the *W* samples, the average mass for each degradation time point was compared to the initial average mass.

3.5.3 Size

The wall thickness and the sample width of all *C* samples were measured using a Leica DFC280 stereo microscope. To determine the wall thickness (values between 0,6 and 1,35 mm, standard deviation of 0,067 mm), the samples were set under the microscope with a vertical spinning axis: Two magnified photos of each side were taken (4x magnification), after which three wall thickness measurements were taken on each photo and all 12 measurements were averaged.

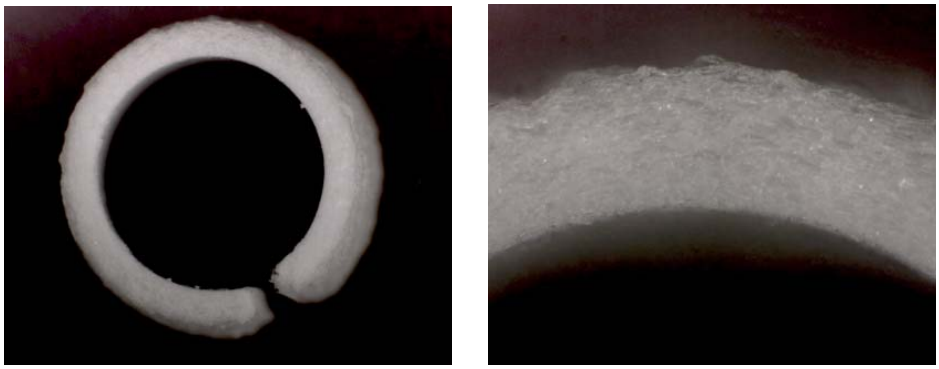

Figure 3.6 Stereo microscope images of sample C14-6

For the measurement of the sample width (values between 9,38 and 10,16 mm, standard deviation of 0,104 mm), each sample was rolled open and fixed between two glass microscopy slides. The sample width was measured 5 times under the microscope and the sample length (values in the range of 17,57-19,9 mm, standard deviation of 0,205mm) was measured 3 times with a ruler. All measurements were averaged.

3.5.4 Tensile properties

The *C* samples were rolled open and clamped at each cross-head on an Instron 5544 universal testing machine with a 500N load cell (both Instron, Norwood, USA) using custom made clamps which are illustrated in Figure 3.7.

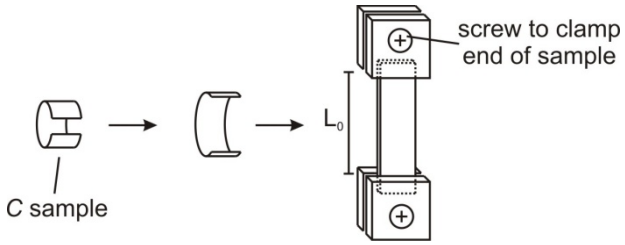

Figure 3.7 Clamping system for tensile testing

On each end of the sample 2-3 mm of the sample length were clamped. The resulting gauge length L_0 varied between 9,90 and 11,58 mm and was measured for each sample.

The tensile testing based on the fact that healthy human arteries experience 3-10% strain [9]. To ensure that the samples bear the cyclic loading of the pulsatile flow, all samples were pre-loaded with 5 tensile pre-cycles up to 20% strain. Thereafter all samples were loaded to failure. The whole testing procedure was conducted with a cross-head speed of 20 mm/min. Based on the gauge length L_0, the average wall thickness and the average width of each sample, stress-strain data was produced.

3.6 Analysis procedure and statistics

To determine the linear elastic modulus of the circumferential samples, a straight line was fitted into the rise of each stress strain graph. Within the first 20% this line was oriented along the rise of the initial precycle to enable comparability with data achieved by tensile testing without preconditioning. For higher strains, the line was continued with the same slope as long as it matched visually with the stress strain graph. The gradient of this line represents the linear elastic modulus. The linear elastic limit –represented by the top end of the line - was determined and the maximum tensile stress after preconditioning was extracted together with the corresponding tensile strain (see Figure 3.8). All of these values were averaged within each degradation group. To analyse the preconditioning, the maximum stresses of the precycles of each sample were extracted (see Figure 3.8). The decrease in these stresses was analysed by comparing the maximum stress of each precycle with the maximum stress of the previous precycle. The resulting decreases in stress were averaged within the corresponding degradation group.

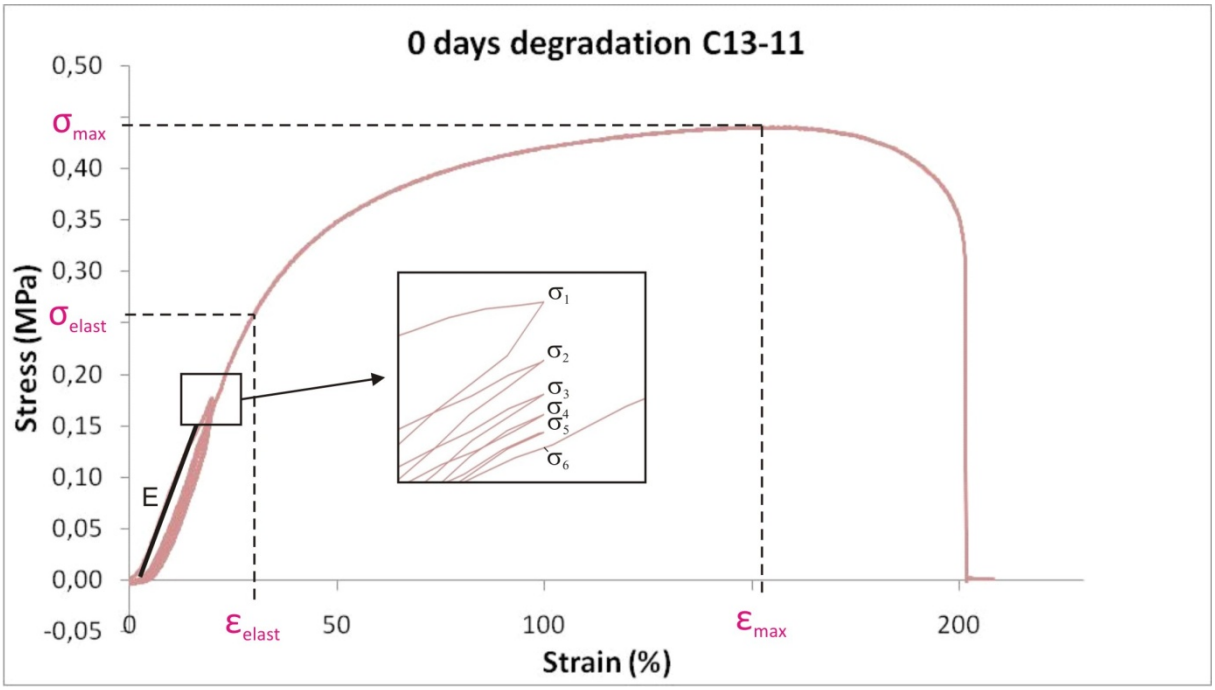

Figure 3.8 Representative stress-strain characteristics of a non degraded sample

Statistical analysis was performed by Hugo Krynauw using "Statistica" software. The Tukey-Kramer Honestly Significant Difference (HSD) was applied to determine statistically relevant changes compared to the initial value. α was set to 0.05 to achieve a confidence coefficient –

which is represented by 1-α – of 0.95. The variance of all values was reviewed and expressed by error bars. These error bars represent 95% statistical confidence of the values.

Several series of measurements were reviewed and tested for statistical significant changes compared to the initial value:

- The maximum stress and the stress at the linear elastic limit versus degradation time;
- The maximum strain and strain at the elastic limit versus degradation time;
- The linear elastic modulus E versus degradation time;
- The stress drops between the precycles as fraction of □□□versus degradation time;
- The fraction (□□□□□□□□(□□□□□□□□versus degradation time;
- The mass loss percentage versus degradation time.

Chapter 4 Results

This chapter presents the results of the tensile testing, mass loss study and SEM analysis.

4.1 Tensile testing

To illustrate the changes occurring during degradation, Figure 4.1 shows stress strain curves and Figure 4.2 a zoom on the corresponding precycles for 0, 22 and 34 days of degradation.

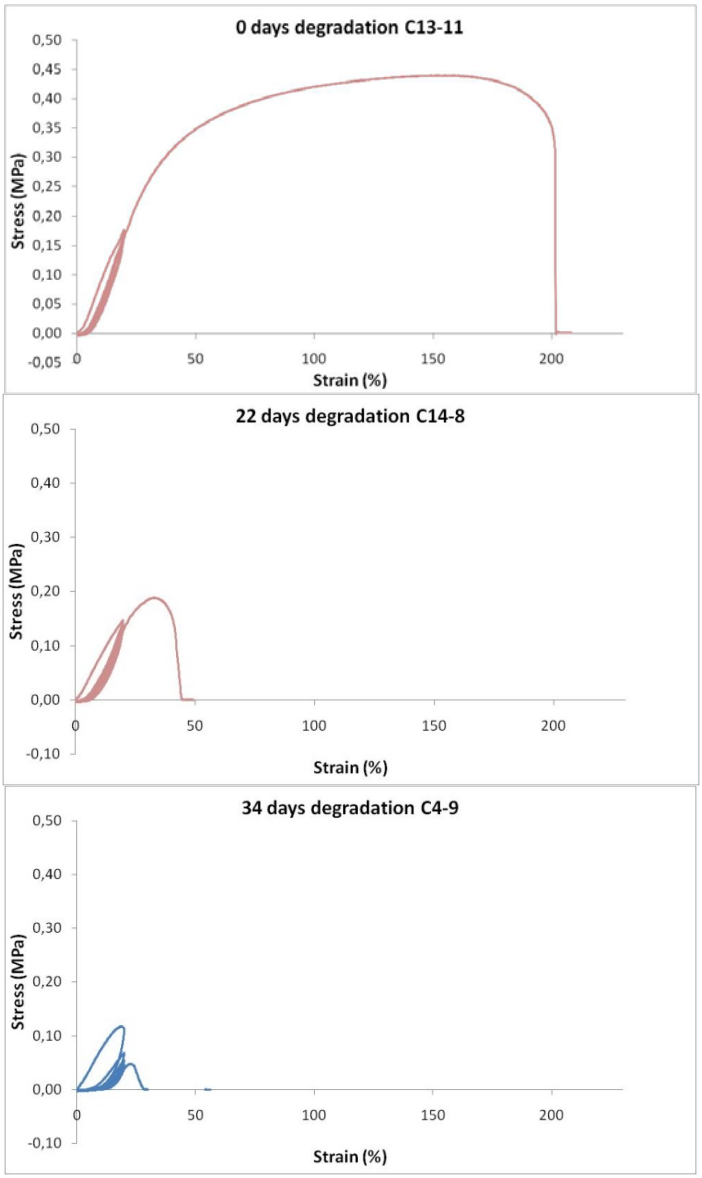

Figure 4.1 Stress strain curves for 0, 22 and 34 days of degradation

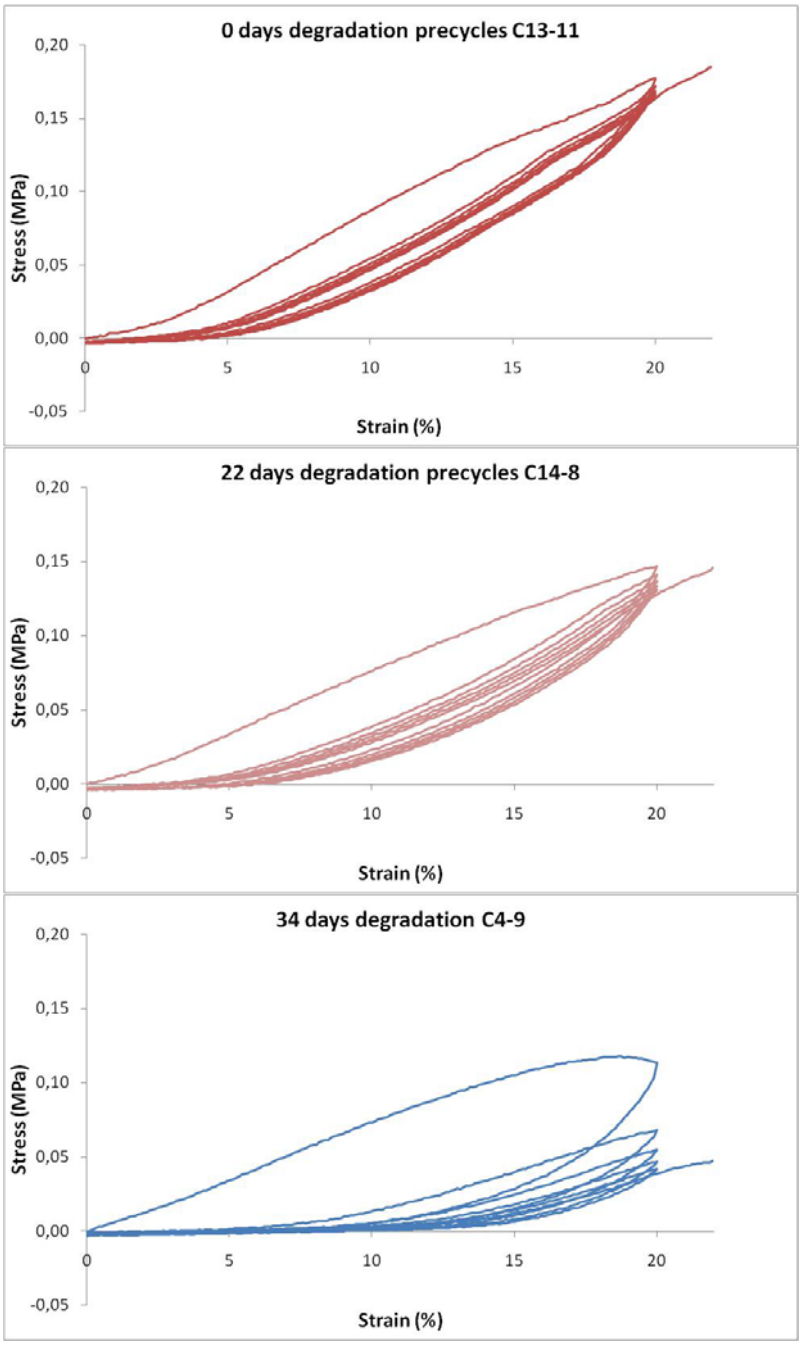

Figure 4.2 Precycles for 0, 22 and 34 days of degradation

Regarding the statistical analysis of all samples, the maximum stress and the stress at the linear elastic limit showed similar, overall decreasing tendencies (see Figure 4.3). They seemed to increase during the first 5 days of degradation and to decrease between 5 and 34 days of degradation. According to the statistical analysis, however, the increase during the first 5 days of degradation was not significant. For degradation times longer than 5 days, changes in the maximum stress were significant and for degradation times longer than 14 days changes in the elastic limit were significant. Within the first 30 days of degradation the maximum stress was higher than the stress at the linear elastic limit. After 34 days of degradation the maximum stress was lower than the stress at the linear elastic limit, however, the relevance of these relative positions was not reviewed statistically. The variation of the stress, represented by the error bars, was different for each time point of degradation. Both, the maximum stress and the linear elastic stress showed a comparable big variance during the first 14 days and at 26 days of degradation.

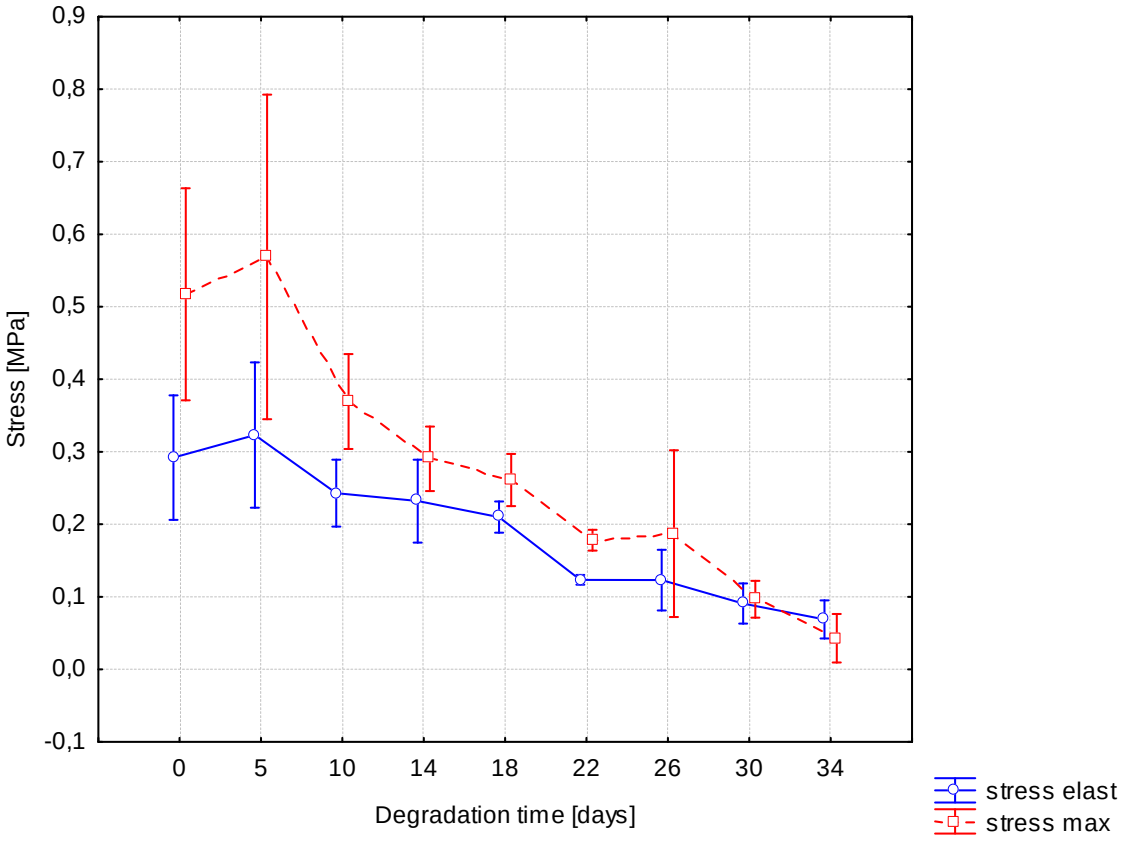

Figure 4.3 Maximum stress and linear elastic stress vs. degradation time (95% confidence)

Regarding the strain of the linear elastic limit and the maximum in Figure 4.4, an overall decrease was seen for both measures. All changes were statistically significant, except the changes in the linear elastic strain for 5 and 14 days. In all measurements the maximum strain was higher than the strain at the linear elastic limit however the difference of the values decreased during the first 14 days of degradation and was more constant for longer degradation times. The maximum strains of 0, 5, 10 and 34 days degradation showed a comparable high variance, whilst all other strains had a small error.

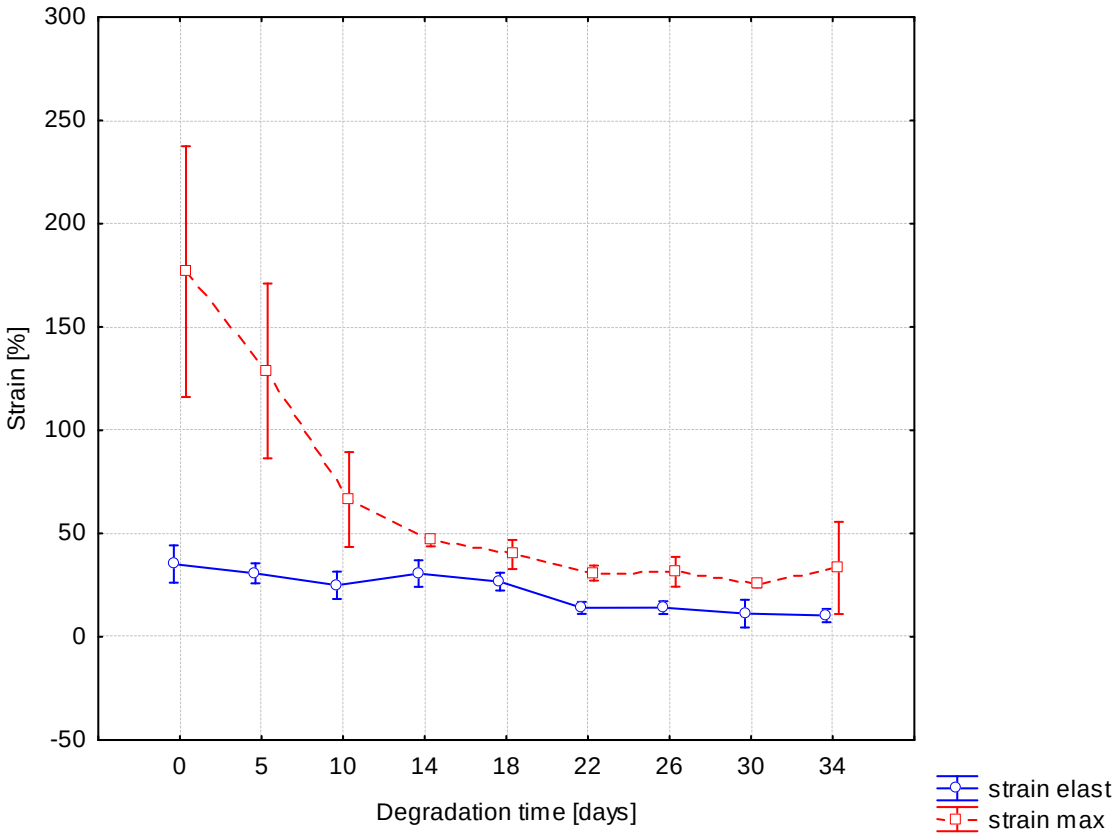

Figure 4.4 Maximum strain and linear elastic strain vs. degradation time (95% confidence)

The values of the linear elastic modulus (E) versus degradation time showed no clear tendency and no statistically relevant changes. The averaged values of E for the different degradation time points varied between 0,7 and 1,1 MPa and had a high variance compared to the changes in the mean values - especially the values for 5, 26 and 30 days of degradation.

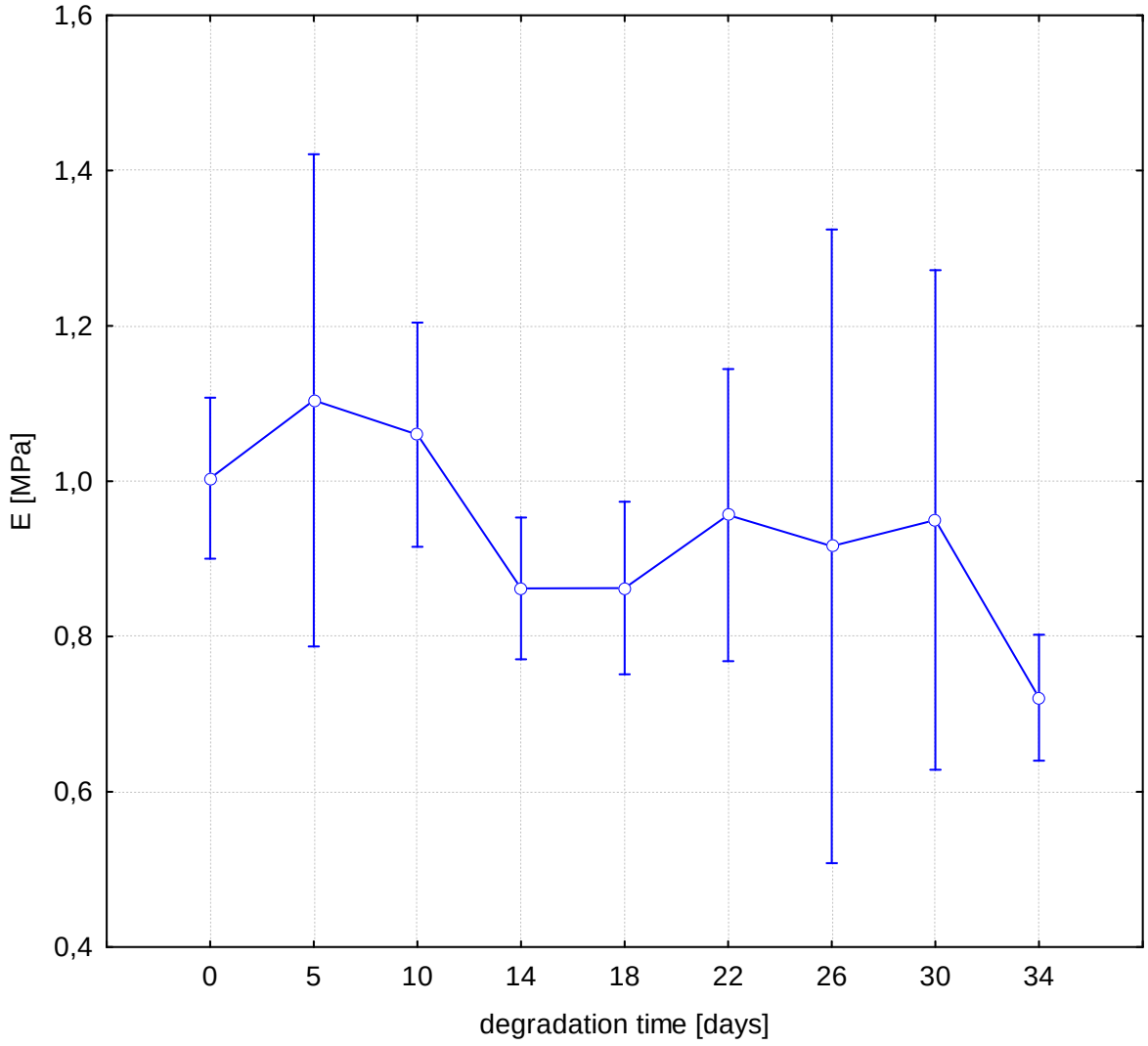

Figure 4.5 Linear elastic modulus (E) vs. degradation time (95% confidence)

The maximum stress of each precycle was extracted for all samples. For each degradation time point the values were averaged and the standard deviation was determined. The results are summarized in Table 4.1.

[redacted]

Table 4.1 Averaged maximum stress of precycles vs. degradation time

To illustrate the changes occurring during precycling and degradation, the averaged maximum stress of precycle 1 to precycle 6 for 5, 22 and 34 days of degradation were plotted in Figure 4.6.

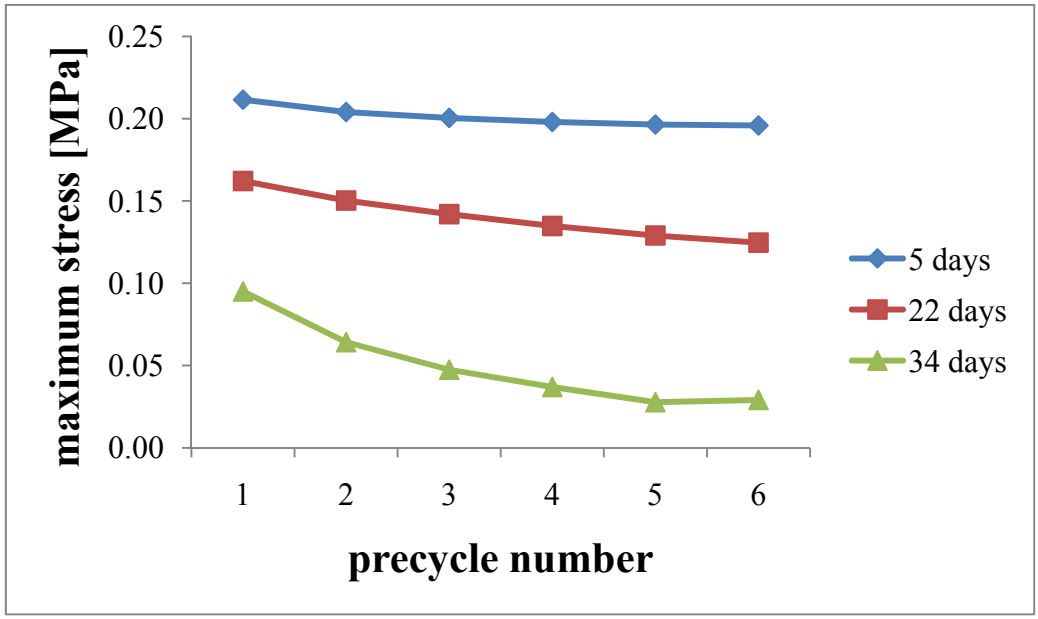

Figure 4.6 Tendencies in max. precycle stress for 5, 22 and 34 days of degradation

The curves plotted in Figure 4.6 are only meant to give a first impression of the changes happening. Further analysis and evaluation of the data will be done in the discussion.

4.2 Mass loss

Analysing the mass measurements, no statistically significant changes versus degradation time were noticed. The mass loss percentage varied between 0 and 0,8%. The variance was high compared to the changes in the mean values.

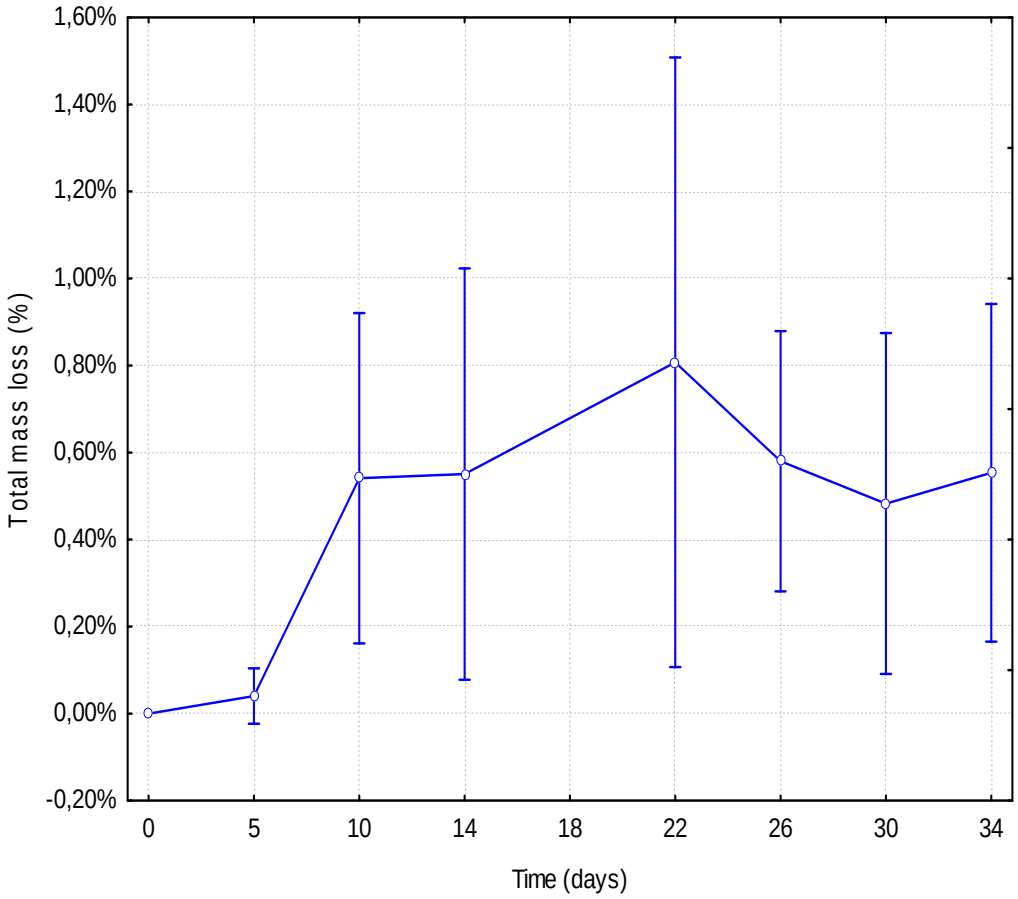

Figure 4.7 Mass loss compared to initial mass vs. degradation time (95% confidence)

4.3 SEM images

The structure of each graft was analysed by means of a SEM. The resulting images showed that the fibres had diameters between 1 and 20 □m, they were slightly oriented and moderately merged. The following figure shows an SEM image of sample S12-1 taken at a magnification of 200x.

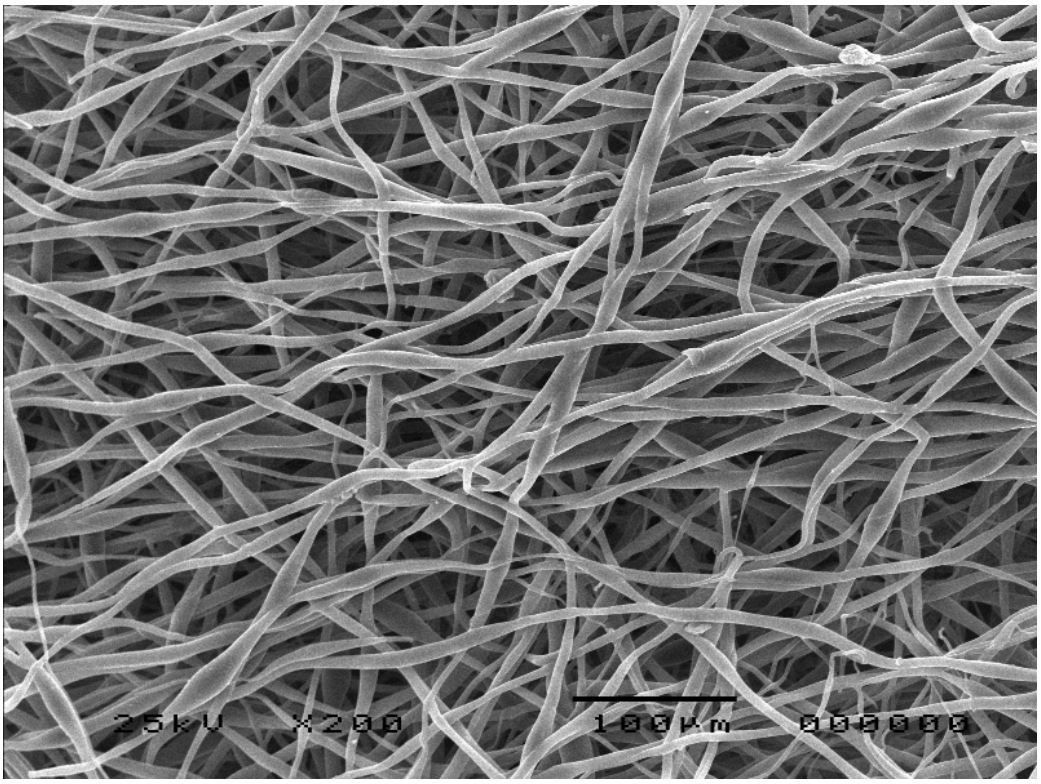

Figure 4.8 SEM image of sample S11-1, 0 days degradation

At a magnification of 7500x a smooth wave-like surface of the fibres could be observed. Comparing fibre surfaces for 0, 14 and 34 days of degradation, no obvious differences appeared.

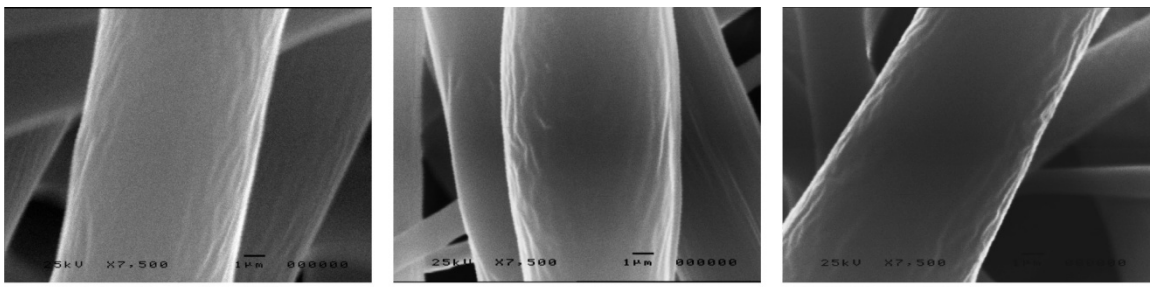

S12-1, 0 days degradation S3-2, 14 days degradation S4-2, 34 days degradation

Figure 4.9 Fibre surfaces for 0, 14 and 34 days of degradation

After tensile testing to failure, the overall structure of the samples was very similar to the structure of samples which had not been tensile tested. The only change observed were single ripped fibres which still seemed to be close to their original position. Figure 4.10 shows an SEM image of sample C3-6 after tensile testing to failure. Some of the ripped fibres are marked with a circle.

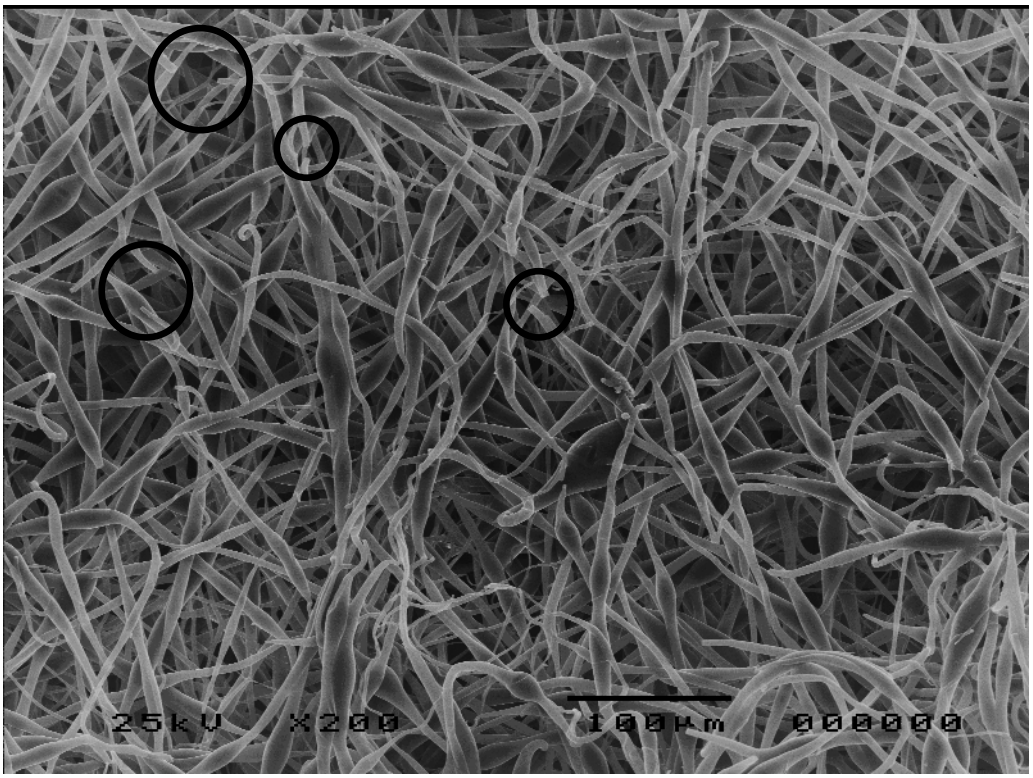

Figure 4.10 SEM image of sample C3-6 after 5 days of degradation and tensile testing to failure

Chapter 5 Discussion

5.1 Introduction

Considering the application as a vascular graft, this discussion will in particular focus on the material's behaviour after cyclic preloading. It first looks at the overall mechanical behaviour and then discusses the changes occurring during degradation.

This discussion is based on values which possibly contain errors due to:

- Imprecision of the electro-spinning process (changes in temperature and humidity, evaporation of the solvent during the spinning process, or loss of material due to spinning towards the wall of the box);
- Imprecision of the measurement equipment (scale, microscope, tensile testing machine);
- Imprecision of the visual judgement (linear elastic curve fitting, determination of σ_{elast} and ε_{elast}).

These errors are difficult to quantify, however they contribute to the statistically determined variances and therefore indirectly stated in the variance of each value.

5.2 The overall mechanical behaviour

Regarding the stress-strain curves of the initial samples (0 days degradation), a clear similarity to the Mullins effect can be observed (compare Figure 2.5 and Figure 4.2). The Mullins effect was originally observed for filled rubbers [44], however continuing studies reported the same behaviour for unfilled crystallizing rubbers [38]. DegraPol® is composed of crystalline hard segments and rubbery soft segments (see section 2.4), and can thus be seen as an unfilled crystallizing rubber that exhibits the Mullins effect. Another reason for the mechanical behaviour described above could lie in the structure achieved by electro-spinning. The meshes that were investigated in this study consist of long fibres which are merged on some contact points. Rubbers – when analysed in their molecular structure – show a similar configuration: They consist of long molecules which are connected on some contact points. The electro-spun meshes of this study could be interpreted as a macroscopic version of a rubber structure. To justify both or one of these analogies it could be interesting to compare

electro-spun meshes made of materials showing the Mullins effect with meshes made of materials which do not show the Mullins effect as well as different structures (blocs, meshes, foams,…) made of a material which shows the Mullins effect. This could give information about the different influences of the macroscopic and the molecular structure on the mechanical characteristics.

For the mechanical characterisation it is interesting to find characteristic points on the stress strain curve.

5.2.1 Characteristic points on the stress strain curves

Regarding the cyclic preloading (Figure 4.2) one can see that the precycling changes the material's behaviour. To get information about the material that can be compared to other experiments without precycling or with a different way of precycling, one can look at the rise of the initial precycle, as this part of the curve is not influenced by the cyclic nature of the experimental setup. It is only represented by the elastic modulus E. Looking at the data extracted for E (see Figure 4.5), a variance slightly bigger than in previous studies can be seen (see section 2.7.1). A possible reason for this might be inconsistence in the electro-spun structure of the samples. As explained above, the electro-spun structures examined in this experiment show a rubber-like macroscopic arrangement which probably also influences the elastic behaviour. However the precise configuration of the mesh - the amount of merging and the fibre thickness - is not necessarily constant. Even though the spinning parameters were kept constant, changes in ambient parameters like temperature or humidity can influence the resulting electro-spun structure (see section 2.6.2). The elastic behaviour of the structures can therefore vary and lead to the variance in E. Due to this variance small changes during the degradation process can hardly be captured and will be reported as statistically insignificant. Variations in the electro-spun structure might also be the reason for the big difference to the values for E observed in previous studies which were conducted without precycling (see section 2.7.1). Going back to the characterisation of the stress-strain behaviour, the elastic modulus thus seems to be difficult to compare in a representative way.

Another characteristic point on the stress-strain curves is the point of the maximum stress. This maximum is measured after the precycling and is therefore different from a maximum measured on a sample without precycling. However, considering the cyclically loaded application of the structures, the maximum stress after preconditioning is more relevant than

the maximum stress without preconditioning. To judge the long term stability of the measured maximum stress, it is important to know if the material is completely conditioned, or if it will still change its properties in a cyclically loaded application. Before discussing the maximum stress and strain, one should therefore evaluate the state of conditioning. This can be done by analysing the precycles.

5.2.2 The state of conditioning

Material conditioning is known as the adaptation of a material to cyclic stress. For many materials which also show the Mullins effect, the conditioning occurs during the first few (up to 10) cyclic loadings [38]. After that the material exhibits stable mechanical behaviour for continued cyclic loading and is called conditioned. To analyse the state of conditioning in this experiment, the stress drops between the maximum values of the precycles (see Table 4.1) were extracted as a fraction of σ_1 and plotted in Figure 5.1.

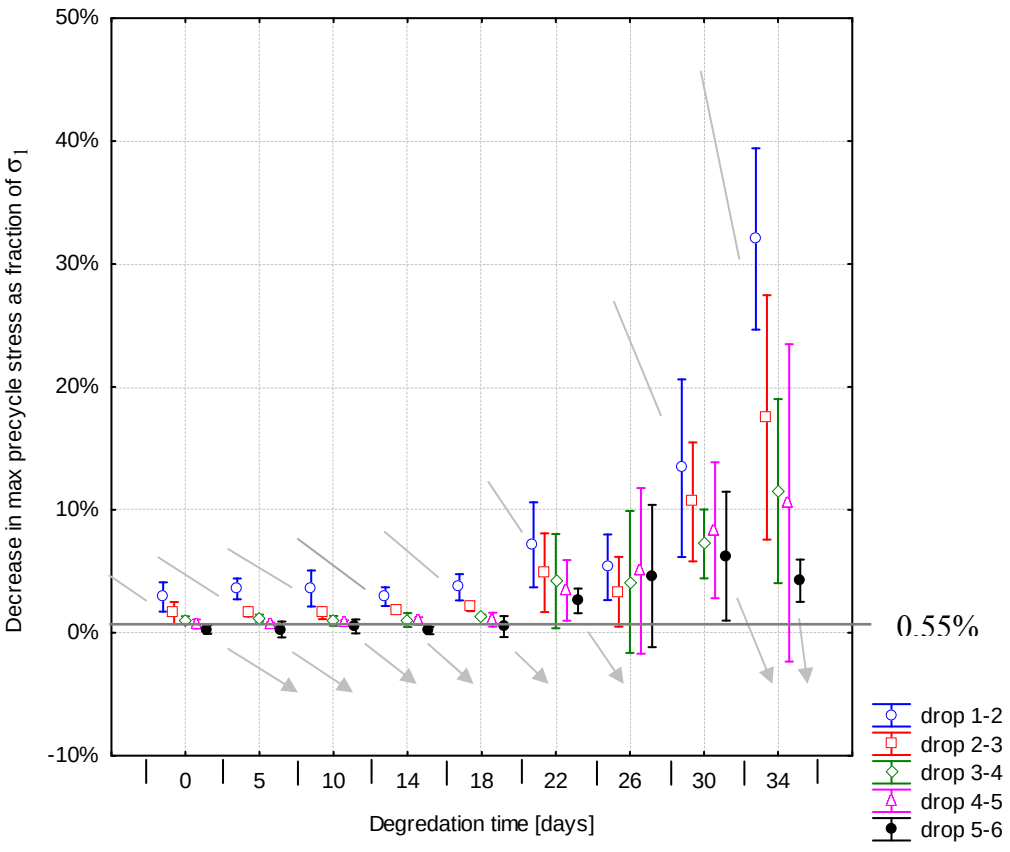

Figure 5.1 Decrease in max. precycle stress as fraction of σ_1 vs. degradation time (95% confidence)

For every single degradation time point 5 different stress drops are observed. These stress drops decrease during precycling. The decreasing trend – illustrated by arrows - indicates

ongoing conditioning. If the stress drop is 0 MPa, conditioning within the loading range is complete. Regarding the stress drops versus degradation time (Figure 5.1) one can see that drop 5-6 is stable and very close to 0% for degradation times ≤ 18 days. For longer degradation times the values for drop 5-6 vary. This change in the trend leads to the assumption that the conditioned state is reached for drops below 0.55%, but not for higher values. The results of this experiment report values close to 0, but not exactly 0. To know which difference is tolerable with respect to the conclusion that the material is conditioned, the decreasing tendency in the stress drops was analysed by comparing drop 5-6 to drop 1-2 (see Figure 5.2). If the drop comparison results in a small value, the stress drops have a strongly decreasing tendency. Assuming that this tendency will continue, samples with a small value for the drop comparison – and hence a strong decreasing tendency of the stress drops – are very close to their conditioned state, even if the last stress drop fraction is not exactly 0. Regarding the stress drop comparison for this experiment (Figure 5.2) one can see that the values are comparable low – and therefore strongly decreasing - for degradation times ≤ 18 days. After that, the values are higher and exhibit a comparable high variance.

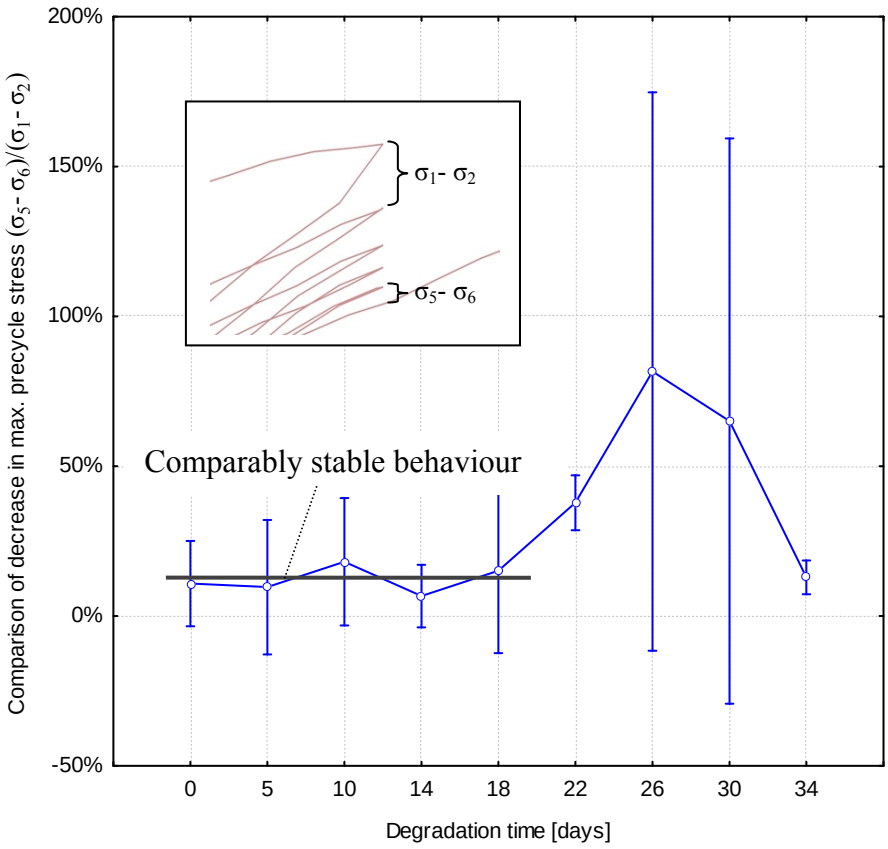

Figure 5.2 Comparison of decrease in stress ($\sigma_5 - \sigma_6$)/($\sigma_1 - \sigma_2$) vs. degradation time (95% confidence)

Based on these observations, the samples examined in this study are considered preconditioned if they degraded for 18 or less days.

Keeping these results about the preconditioning in mind and going back to the maximum stress (Figure 4.3), one can state that the maximum stresses for 18 or less days of degradation are stable characteristics of the conditioned material.

The fact that the conditioned state is not reached for 22 or more days indicates that there are significant changes occurring during the degradation process. In order to discuss these changes, the following section will compare different degradation time points.

5.3 Changes occurring during degradation

5.3.1 Analysis of the degradation steps

In order to understand what is happening as the material degrades it is important to remember the degradation process. As described in section 2.3.3 hydrolytic degradation occurs in two steps: First, the macromolecular chain is broken while the sample mass remains unaltered. When the chain fragments are small enough to permeate into the aqueous medium, the second step of degradation starts and mass loss can be observed [22]. The fact that the mass loss percentage presented in Figure 4.7 does not show significant increases leads to the conclusion that all samples examined in this study are still within the first step of degradation. This conclusion is also supported by the SEM analysis. The fibre surfaces of different degradation time points are very similar. No changes in the surface due to loss of material can be seen. Bearing this fact in mind, all changes in the material can now be interpreted as a result of mainly hydrolytic cleavage but no loss of material.

5.3.2 Influence of the degradation process on the stress-strain characteristics

To understand, how this first degradation step influences the stress/strain characteristics of the material, it is important to consider the molecular structure of DegraPol®. As explained in section 5.2, the molecular structure of DegraPol® can be described as a mesh of molecular chains which contain soft and hard segments. These chains are arranged in a manner that a continuous amorphous matrix is formed in which the crystals are dispersed.

During the first degradation step of this structure, the polar ester bonds in the molecular chains are cracked by hydrolysis (see Figure 5.3).

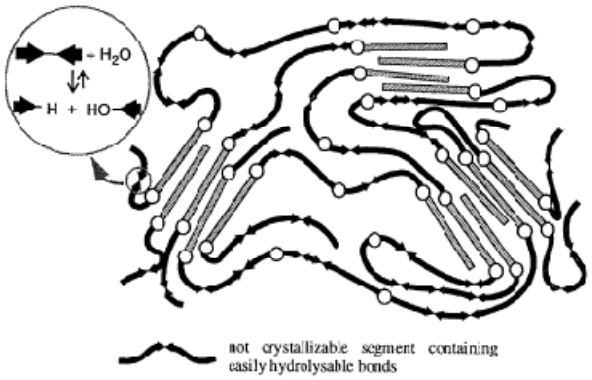

Figure 5.3 Hydrolytic cracking scheme for DegraPol®, [23]

Zooming out to look at the electro-spun mesh, a crack in the molecular chain of the polymer can be seen as a little defect in the electro-spun fibre. If the fibre is now stretched, the stress will be locally increased in the area around this defect. Stretching the fibre even more and thus increasing the overall stress, the critical stress for failure will be reached earlier in the area around the defect compared to the rest of the fibre. The fibre will therefore start breaking at this point with a lower maximum stress compared to a fibre without a defect. The longer the samples degrade, the higher the density of the defects and thus the lower the linear elastic and the maximum stress. This explains the overall decreasing trend of σ_{elast} and σ_{max} which is seen in Figure 4.3. The fact that σ_{max} is lower than σ_{elast} at 34 days of degradation will be explained later.

Going back to the molecular model of DegraPol® and the degradation process, one can also explain the decrease of ε_{max} during degradation. On a molecular level conditioning of thermoplastic elastomeric structures such as DegraPol® can be explained with the aligning of the molecules whilst plastic damage can be seen as the sliding of single molecules which allows the material to stretch further. The failure of the material happens when the molecules are finally separated or ripped. When the material has been degraded, some of the molecules are cracked into smaller pieces. Due to the shorter molecular length less elongation is needed to separate the molecules and hence crack the fibres of the mesh. This explains the decrease in ε_{max} versus degradation time, which is observed in Figure 4.4.

The decrease of ε_{elast} - which marks the onset of plastic damage - versus degradation time (see Figure 4.4) is linked to the decrease of σ_{elast}. As the elastic modulus does not show significant changes during degradation, the overall decrease in σ_{elast} provokes an overall decrease in ε_{elast}. As ε_{elast} gets lower than 20%, not only conditioning, but also plastic damage is occurring

during the cyclic preloading. When the final tensile test to failure starts, the sample has already experienced plastic damage. Some of the molecules are already separated and cannot contribute to the ultimate tensile strength anymore therefore the value for σ_{max} is decreased. If the amount of plastic damage happening during the cyclic preloading reaches a critical value, σ_{max} can be even lower than σ_{elast} since σ_{elast} is taken during the first cycle. As Figure 4.3 shows, this critical value of plastic damage during precycling is reached between 30 and 34 days of degradation. For 30 days of degradation, σ_{max} is still higher than σ_{elast}, whilst for 34 days of degradation σ_{elast} is higher.

Going back to Figure 4.4, one can see that ε_{elast} turns smaller than 20% for degradation times $\geq$ 22 days. This means that plastic deformation happens during precycling if the samples have degraded for 22 or more days. Keeping this in mind and regarding the stress drops of the precycles again, a change in behaviour can be seen after the onset of plastic damage during precycling (see Figure 5.4).

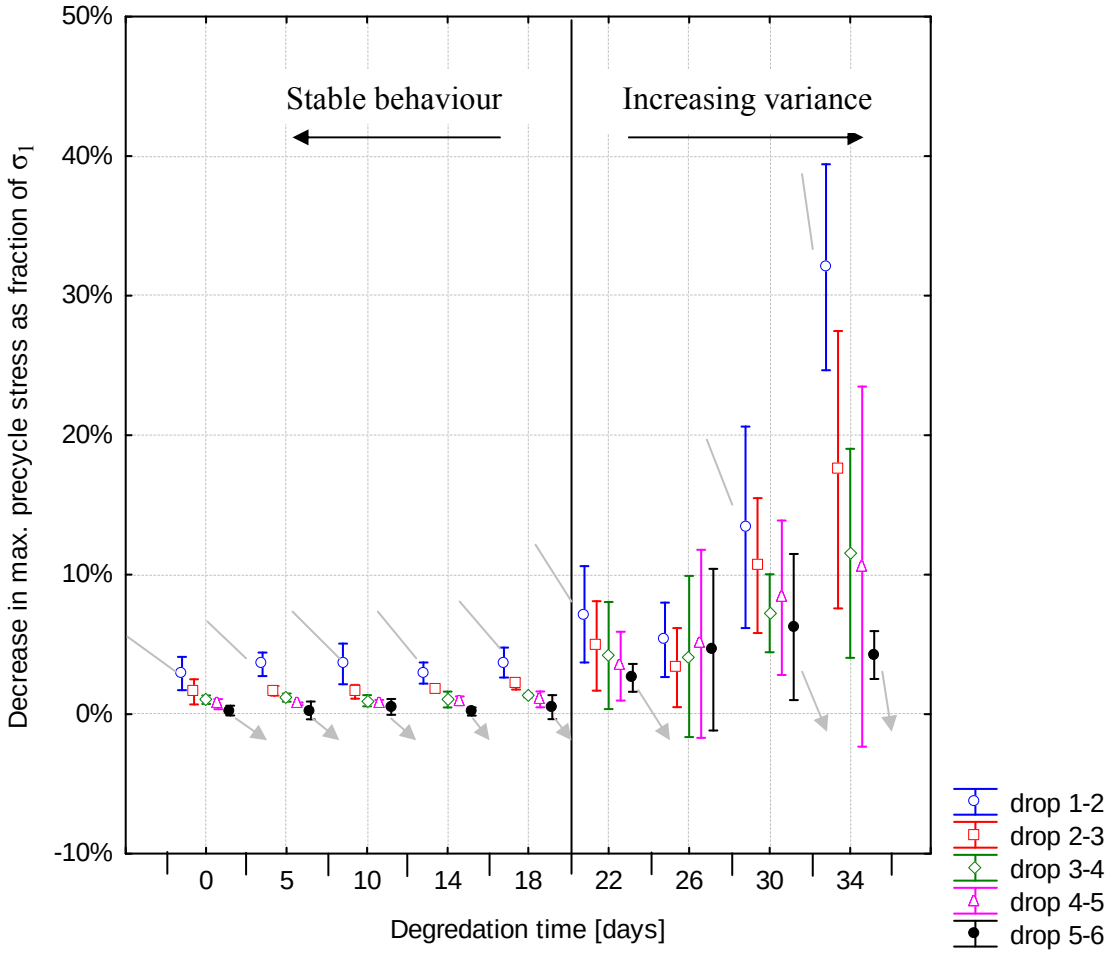

Figure 5.4 Variance trends in stress decrease vs. degradation time (95% confidence)

One can see that the stress drops are stable during the first 18 days of degradation, but increase for longer degradation times. The stability of the values for degradation times ≤ 18 days – when only conditioning but no plastic damage happens during degradation - motivates the assumption that preconditioning is a stable process which seems to be not influenced by degradation.

One can also notice that the variance of the values also increases with increasing plastic damage during precycling. This brings up the impression that plastic damage – described earlier on as the sliding of molecules – is a comparably random process which can lead to very different results in structure and therefore to a high variance observed in Figure 5.4.

The amount of plastic damage during precycling also influences the decreasing tendency of the maximum stress of the precycles (Figure 5.2). For degradation times of 22 and 26 days, when plastic deformation during precycling happens, the stress drop comparison increases. This indicates that the converging trend in the precycles decreases due to increasing plastic damage. Based on these observations, one could now expect the drop comparison to keep increasing for longer degradation times and hence more plastic damage during precycling. For 30 and 34 days of degradation, however, the drop comparison decreases again. This can be explained with the large amount of plastic damage happening during precycling. Due to the plastic damage the samples get longer. If a lot of plastic damage occurs, the sample gets long enough to hardly be stressed as the precycles continue pulling the sample up to 20% strain of the original gauge length. This can be a reason why the stress drops show a decreasing tendency for 30 and 34 days of degradation, even though the plastic deformation is comparable high for these samples.

5.4 Conclusion

In summary, the samples examined in this study reach a preconditioned state if they are degraded for 18 or less days. During the degradation process σ_{max}, ε_{max}, σ_{elast} and ε_{elast} decrease. For degradation times longer than 18 days ε_{elast} is lower than 20%, plastic damage happens during precycling and the samples do not reach a preconditioned state.

With respect to the cyclic loading of a vascular graft, the material can only be characterized for degradation times up to 18 days, as it does not reach a preconditioned state for longer times of degradation. The key parameter for judging the ability of the material to withstand the cyclic stress seems to be ε_{elast}. As long as the overall maximum strain in the graft is lower than this parameter, the material will reach a preconditioned state. When preconditioning is achieved the corresponding values for σ_{max} can be seen as stable values describing the maximum stress of the material for cyclically loaded applications.

5.5 Recommendations

As discussed above the structure examined in this study withstands the cyclic stress of pulsatile flow within the first 18 days of degradation. To judge if this structure is applicable as a vascular graft one needs to find out, if the growing cells are strong enough to be loaded gradually after maturing for 18 days. Depending on the result the reinforcement structure can be adapted to achieve an increased mechanical strength of the overall graft. To adapt the mechanical strength, a change in the electro-spinning parameters can also be considered however, there seem to be just little combinations of spinning parameters resulting in a stable Taylor cone and hence a reproducible structure. In the final application the mechanical behaviour of the whole graft is influenced by both structures – the electro-spun mesh and the reinforcement structure - and might therefore differ from the mechanical behaviour examined in this study. More experiments examining different combinations of electro-spun layers and reinforcement structures need to be done to find the solution which best suits for the application as a vascular graft.

For processing and quality control of vascular grafts it would be helpful to describe the change in mechanical properties during degradation as a function of the initial mechanical properties. The characterisation of an undegraded sample could then provide sufficient information to conclude the final mechanical behaviour *in vitro*. In order to develop the

function described above, it would also be necessary to study whether the contamination with water provokes any general changes apart from hydrolysis. This could be done by comparing samples which never touched water with samples that have been contaminated with water for a very short period of time so that the effect of hydrolysis is small.

Keeping in mind that healthy human arteries experience up to 10 % strain [9], one could examine whether the same material stretched only to 10% instead of 20% elongation, will reach a preconditioned state, which exhibits the same maximum stress. This would give an idea of the range, in which the material's characteristics determined in this experiment are relevant.

A third continuative experiment could be the comparison of foams and electro-spun meshes made of materials showing the Mullins effect with foams and meshes made of materials which do not show the Mullins effect. The results of precycling and tensile testing these structures could validate or negotiate the analogy of electro-spun structures and the molecular arrangement in rubbers, which was mentioned in section 5.2. This could give general information about the different influences of the macroscopic and the molecular structure on the mechanical characteristics.

Chapter 6 Summary

Based on the literature review it was found that electro-spun DegraPol® is suitable for cyclically loaded applications like cardiovascular tissue regeneration [11, 12, 25, 27]. The samples were hence made of electro-spun DegraPol® with spinning parameters similar to previous studies to ensure comparability of the results [25]. The samples were degraded in distilled water for 0, 5, 10, 14, 18, 22, 26, 30 and 34 days. Mass loss studies were conducted, the microstructure was analysed using SEM and the tensile properties were determined with five cyclic pre-loadings to 20% strain and a final tensile test to sample failure. For each of the samples examined the linear elastic modulus (E), the stress/strain at the linear elastic limit (σ_{elast}/ ε_{elast}), the maximum stress (σ_{max}) and the corresponding maximum strain (ε_{max}) as well as the maximum stress of each precycle (σ_1- σ_6) were extracted and statistically analysed.

The mass loss study and the SEM analysis showed that all samples were still within the first step of degradation and changes during degradation are a result of mainly hydrolytic cleavage but no loss of material. Based on the stress-strain graphs it was found that the samples exhibit the Mullins effect. In addition statistical analysis showed that σ_{max}, ε_{max}, σ_{elast} and ε_{elast} decreased during degradation due to increasing hydrolytic cleavage. Analysis of the stress decrease during precycling lead to the conclusion that the samples reached a preconditioned state during precycling if they degraded for 18 or less days. This was interpreted as a result of the decrease in ε_{elast}. For degradation times longer than 18 days, ε_{elast} was lower than 20% strain of L_0, plastic damage happened during precycling, the samples did subsequently not reach a preconditioned state and the material would fail under the cyclic loading of the pulsatile blood flow.

For the biomechanical modelling of degradable vascular grafts σ_{max}, ε_{max}, σ_{elast} and ε_{elast} can be used as the material's characteristic if the sample degraded for 18 or less days as the preconditioned state is reached for these degradation times.

With regard to the final application more experiments examining different combinations of electro-spun layers and reinforcement structures need to be done to find the solution which best suits for a vascular graft. This thesis has to be regarded as a starting point and a first approach in order to find and characterize the key parameters to judge the applicability of the structures that were produced.

Chapter 7 Bibliography

1. Department of Health and Human Services, C.f.d.C.a.P., *Chronic Disease Overview - Leading Causes of Death, UK, 2005, Number of deaths.* Stand 20.11.2008.
2. Frieden, T.R., et al., *Public health in New York City, 2002-2007: confronting epidemics of the modern era.* Int. J. Epidemiol., 2008. **37**(5): p. 966-977.
3. Murray, C.J.L. and A.D. Lopez, *Alternative projections of mortality and disability by cause 1990-2020: Global Burden of Disease Study.* The Lancet, 1997. **349**(9064): p. 1498-1504.
4. Murray, C.J.L. and A.D. Lopez, *Mortality by cause for eight regions of the world: Global Burden of Disease Study.* The Lancet, 1997. **349**(9061): p. 1269-1276.
5. Niklason, L.E., *Medical Technology :Replacement Arteries Made to Order.* Science, 1999. **286**(5444): p. 1493-1494.
6. Veith FJ, M.C., Sprayregen S, Montefusco C., *Preoperative saphenous venography in arterial reconstructive surgery of the lower extremity.* Surgery, 1979.
7. Laurencin, N., *Nanotechnology and Tissue Engineering - The scaffold.* Buch, 2008.
8. http://www.med-ed.virginia.edu/courses/cell/handouts/images/BloodVessel_1.gif, *The layers of arteries* 15.02.2010.
9. Conti, J., Strope, ER, *Radial Compliance of Natural and Mock Arteries: How This Property Defines the Cyclic Loading of Deployed Vascular Stents.* Biomedical Science Instrumentation, 38, 2002: p. pp. 163-172.
10. Lin, K., et al., *Reducing electrospun nanofiber diameter and variability using cationic amphiphiles.* Polymer, 2007. **48**(21): p. 6384-6394.
11. Henry, J.A., et al., *Structural variants of biodegradable polyesterurethane in vivo evoke a cellular and angiogenic response that is dictated by architecture.* Acta Biomaterialia, 2009. **5**(1): p. 29-42.
12. Vincent, M., et al., *Cyto- and hemocompatibility of a biodegradable 3D-scaffold material designed for medical applications.* Journal of Biomedical Materials Research Part B: Applied Biomaterials, 2009. **91B**(1): p. 109-121.
13. Bezuidenhout, D., *Poros polymeric superstructures as in-growth scaffolds for tissue-engineered vascualr prostheses.* 2001.
14. Deon Bezuidenhout, N.D., Peter Zilla, *Effect of Well Defined Dodecahedral Porosity on Inflammation and Angiogenesis.* ASAIO Journal 2002; 48:465–471., 2002.
15. Boyan, B.D., et al., *Role of material surfaces in regulating bone and cartilage cell response.* Biomaterials, 1996. **17**(2): p. 137-146.
16. Flemming, R.G., et al., *Effects of synthetic micro- and nano-structured surfaces on cell behavior.* Biomaterials, 1999. **20**(6): p. 573-588.
17. Sandip Sarkar, T.S.-R., George Hamilton, Alexander M. Seifalian, *Achieving the ideal properties for vascular bypass grafts using a tissue engineered approach: a review.* 2007.
18. Grizzi, I., et al., *Hydrolytic degradation of devices based on poly(-lactic acid) size-dependence.* Biomaterials, 1995. **16**(4): p. 305-311.
19. Nair, L.S. and C.T. Laurencin, *Biodegradable polymers as biomaterials.* Progress in Polymer Science. **32**(8-9): p. 762-798.

20. Suming, L., *Hydrolytic degradation characteristics of aliphatic polyesters derived from lactic and glycolic acids.* Journal of Biomedical Materials Research, 1999. **48**(3): p. 342-353.
21. Kim, K., et al., *Control of degradation rate and hydrophilicity in electrospun non-woven poly(,-lactide) nanofiber scaffolds for biomedical applications.* Biomaterials, 2003. **24**(27): p. 4977-4985.
22. Andreas, L., et al., *Hydrolytic Degradation of Phase-Segregated Multiblock Copoly(ester urethane)s Containing Weak Links.* Macromolecular Chemistry and Physics, 2001. **202**(13): p. 2702-2711.
23. Andreas, L., N. Peter, and W.S. Ulrich, *Tissue-compatible multiblock copolymers for medical applications, controllable in degradation rate and mechanical properties.* Macromolecular Chemistry and Physics, 1998. **199**(12): p. 2785-2796.
24. Neuschwander Peter, U.G., Suter Ulrich, Ciardelli Gianluca, Hirt Thomas, Keiser Oliver, Kojima Kazushige, Lendlein Andreas, Matter Sandro *Patent.* 1996.
25. Saad B, K.O., Welti M, Uhlschmid GK, Neuenschwander P, Suter UW., *Multiblock copolyesters as biomaterials: in vitro biocompatibility testing.* J Mater Sci Mater Med, 1997.
26. *DegraPol Homepage, state 11.02.2010.* 2010.
27. Danielsson C, R.S., Simonet M, Neuenschwander P, Frey P., *Polyesterurethane foam scaffold for smooth muscle cell tissue engineering.* Biomaterials, 2006.
28. Henry, 2 Marc Simonet,3 Abhay Pandit,1,2 Peter Neuenschwander3, *Characterization of a slowly degrading biodegradable polyesterurethane for tissue engineering scaffolds.* Wiley InterScience, 2007: p. 669–679.
29. Ivan, M., et al., *Selective differentiation of mammalian bone marrow stromal cells cultured on three-dimensional polymer foams.* Journal of Biomedical Materials Research, 2001. **55**(2): p. 229-235.
30. Lim, S.H. and H.-Q. Mao, *Electrospun scaffolds for stem cell engineering.* Advanced Drug Delivery Reviews, 2009. **61**(12): p. 1084-1096.
31. Riboldi SA, S.M., Neuenschwander P, Cossu G, Mantero S., *Electrospun degradable polyesterurethane membranes: potential scaffolds for skeletal muscle tissue engineering.* Biomaterials, 2005.
32. McManus, M.C., et al., *Mechanical properties of electrospun fibrinogen structures.* Acta Biomaterialia, 2006. **2**(1): p. 19-28.
33. Saad B, K.Y., Welti M, Uhlschmid GK, Neuenschwander P, Suter UW., *DegraPol-foam: a degradable and highly porous polyesterurethane foam as a new substrate for bone formation.* Artif Organs, 2000.
34. Reneker, D.H. and H. Hou, *Electrospinning*, in *Encyclopedia of Biomaterials and Biomedical Engineering*. 2004, Marcel Dekker, Inc. p. 543-550.
35. Takehisa, M., et al., *Mechano-active scaffold design of small-diameter artificial graft made of electrospun segmented polyurethane fabrics.* Journal of Biomedical Materials Research Part A, 2005. **73A**(1): p. 125-131.
36. Doshi, J.a.D.H.R., *Electrospinning process and applications of electrospun fibers.* Journal of Electrostatics, 1995: p. 151-160.
37. Deitzel, J.M., et al., *The effect of processing variables on the morphology of electrospun nanofibers and textiles.* Polymer, 2001. **42**(1): p. 261-272.
38. Diani, J., B. Fayolle, and P. Gilormini, *A review on the Mullins effect.* European Polymer Journal, 2009. **45**(3): p. 601-612.

39. Ryan R. Duling, R.B.D., *Mechanical Characterization of Electrospun Polycaprolactone „PCL…: A Potential Scaffold for Tissue Engineering.* J. Mech. Phys. Solids, 41(2), pp. 389–412).
40. Keunhyung Lee, B.L., Chihun Kim, and Hakyong Kim*, Kwanwoo Kim, Changwoon Nah, *Stress-Strain Behavior of the Electrospun Thermoplastic Polyurethane Elastomer Fiber Mats.* 2005.
41. Hong, Y., et al., *A small diameter, fibrous vascular conduit generated from a poly(ester urethane)urea and phospholipid polymer blend.* Biomaterials, 2009. **30**(13): p. 2457-2467.
42. Frédéric, C., R. Navneeta, and M. Diego, *Macromolecular Biomaterials for Scaffold-Based Vascular Tissue Engineering.* Macromolecular Bioscience, 2007. **7**(5): p. 701-718.
43. Thomas V, Z.X., Catledge SA, Vohra YK., *Functionally graded electrospun scaffolds with tunable mechanical properties for vascular tissue regeneration.* Biomed Mater. 2007 Dec;2(4):224-32. Epub 2007 Oct 8., 2007.
44. L Mullins - J. Rubber Res, *Effect of stretching on the properties of rubber.* 1947.